Geophysical Journal International

Geophys. J. Int. (2025) **242,** 1–25
Advance Access publication 2025 May 2
Research Paper

https://doi.org/10.1093/gji/ggaf151

A missing palaeomagnetic signal in Middle Devonian pillow lavas

R.A. de Boer [1], L.V. de Groot [1], M.J. Dekkers,[1] P. Königshof[2] and A. van der Boon[3]

[1] *Palaeomagnetic Laboratory Fort Hoofddijk, Department of Earth Sciences, Utrecht University,* 3584 *CD, the Netherlands. E-mail: r.a.deboer1@uu.nl*
[2] *Historical Geology and Facies, Senckenberg Research Institute and Natural History Museum,* 60325, *Frankfurt, Germany*
[3] *Centre for Planetary Habitability, University of Oslo,* 0371, *Norway*

Accepted 2025 April 10. Received 2025 March 31; in original form 2024 October 16

SUMMARY

The configuration of the Earth's magnetic field during the Middle Devonian (394.3–378.9 Ma) is poorly understood. The magnetic signals in Middle Devonian rocks are often overprinted during the Kiaman reverse superchron, obscuring their primary remanence. In other cases, available palaeomagnetic data are ambiguous, conflicting with tectonic reconstructions or dipolar geomagnetic field behaviour. Here, we study the palaeomagnetic signal of Middle Devonian pillow basalts from the Rhenish Massif in Germany. Our rock-magnetic experiments show that the pillow basalts can store and retain magnetizations over time. However, the pillow basalts have a somewhat low initial natural remanent magnetization (NRM), which is not expected based on their magnetite content. The palaeomagnetic directions determined from alternating field demagnetization, thermal demagnetization and a combination of both, fail to cluster around a common mean. Great circle analyses of these palaeomagnetic directions reveal traces of both Kiaman and present-day field overprints. Our palaeointensity measurements have a very low success rate of < 2 per cent, with only one sample yielding a result of 5.9 μT. This low intensity might explain the low initial NRM of the samples and the lack of interpretable directional data in this study. However, given the very low success rate, this result does not convincingly represent the palaeointensity of the Middle Devonian field. All together, the lack of signal in our Middle Devonian pillow lavas could be a sign of an (ultra-)low, or non-dipolar or possibly even absent geomagnetic field during the time of formation.

Key words: Magnetic fabrics and anisotropy; Magnetic field variations through time; Magnetic mineralogy and petrology; Palaeointensity; Palaeomagnetism.

1 INTRODUCTION

The intensity and the reversal frequency of the geomagnetic field vary over timescales from years to millions of years (e.g. Merrill *et al.* 1998). These variations in Earth's magnetic field are caused by processes in the Earth's outer core that drive the geodynamo (Tauxe *et al.* 2018, section 1.9) and potentially by cyclical deep Earth processes (Hawkins *et al.* 2021). However, the behaviour of the geodynamo is largely unpredictable (Driscoll 2016). Understanding geodynamo behaviour is essential for our understanding of Earth's internal evolution. The palaeomagnetic record, which relies on the recording of Earth's magnetic field by rocks, is thus paramount to uncover information on the processes that drive the geodynamo. However, deep Earth processes are less understood before 300 Ma (Hawkins *et al.* 2021), because older rock material is either scarcely available, or has been subject to alteration and metamorphism that could have partially reset or completely overprinted their natural remanent magnetization (NRM).

This is particularly prominent in Devonian rocks where palaeomagnetic research is typically difficult and inconclusive. Devonian rocks are often remagnetized, particularly during the Kiaman reverse polarity superchron (∼318–267 Ma, e.g. Zwing & Bachtadse 2000; Zegers *et al.* 2003; Jelenska *et al.* 2014; Pastor-Galán *et al.* 2015; van der Boon *et al.* 2022). When primary NRMs are argued to be present, palaeomagnetic analyses often produce enigmatic results, which are interpreted as evidence for a hyper-reversing magnetic field or a complex, non-dipolar magnetic field configuration during this time period (Hansma *et al.* 2015; Shcherbakova *et al.* 2017; Shatsillo & Pavlov 2019; Hawkins *et al.* 2021; Shcherbakova *et al.* 2021). Although some studies (e.g. Hansma *et al.* 2015; Green *et al.* 2021) have argued for successfully determined Devonian palaeodirections, the Devonian period is generally suffering from palaeomagnetic data scarcity and an uneven data distribution in time, with a particular scarcity in the Middle and Late Devonian. Because of all ambiguities, only a few robust palaeopoles are determined for the Devonian (e.g. Torsvik *et al.* 2012; van der Boon *et al.* 2022) and the polarity pattern of the Middle-Late Devonian is still undetermined on the geomagnetic polarity timescale (Becker *et al.* 2020). Palaeointensity studies from across the globe mostly suggest low to extremely low intensity values (e.g. Shcherbakova *et al.*

2021). However, not all data pass modern reliability criteria (Bono *et al.* 2022a). Therefore, obtaining new, reliable palaeointensity estimates can strengthen our understanding of the geomagnetic field intensity during the Devonian period. In general, the acquisition of robust palaeomagnetic data, both intensities and directions, can substantially improve our understanding of long-term geomagnetic field behaviour.

Here, we present new palaeomagnetic data from Devonian pillow lavas of the Philippstein quarry (Braunfels, Germany). Since volcanic rocks are more resistant to remagnetization mechanism than sediments, and since these pillow basalts are relatively pristine, we consider them a promising target for finding a preserved primary Devonian magnetic signal.

2 GEOLOGICAL SETTING

The Rhenish Massif (Rheinisches Schiefergebirge) is a fold-and-thrust belt, belonging to the Avalonia terrane (e.g. Franke 2000). During the Devonian, the Rhenish Massif was located on the edge of the Laurussian 'Old Red' continent (Torsvik & Cocks 2004), around a latitude of 20°–25° south of the equator (Marcilly *et al.* 2022; Fig. 1a). The Rhenish Massif predominantly consists of Devonian and Carboniferous rocks, which underwent low grade prehnite-pumpellyite facies metamorphism (Flick *et al.* 1988; Meisl 1995) of Variscan age. Remnants of the Cadomian and Caledonian orogenies are still present in the Massif (Franke 2000). Volcanic activity associated with an extensional setting occurred during the Devonian and Carboniferous (Flick & Nesbor 1988; Nesbor 2019). Magma erupted along fault planes of half grabens formed in this extensional environment (Moe 2000). During the Devonian, volcanic successions of several hundreds of metres thick were formed with diameters reaching up to 10 km. Thinning of the continental crust led to the development of several shallow marine basins and formed the Rhenohercynian basin (Schnapperelle *et al.* 2021) where thick successions of siliciclastic sediments accumulated (Königshof *et al.* 2010).

The rock samples for this study were collected in the Philippstein quarry (50.475°N, 8.374°E, Fig. 1b), which exposes part of a thick sequence of basalts from a submarine volcano of Givetian age (Nesbor 2007). The geochemical signature of the volcanic rocks reveals an intraplate volcanic environment (Wedepohl *et al.* 1983; Flick & Nesbor 1988; Nesbor 2019). At the base of the Philippstein quarry, alkaline basaltic lavas are exposed, which are nowadays no longer accessible due to quarry infilling. These lavas form a coherent cooling unit with vertical columnar jointing (Königshof *et al.* 2010). The succession continues with ash tuffs, hyaloclastites and pillow fragment breccias, overlain by a thick succession of pillow lavas (Nesbor 2007). The Philippstein pillow basalts are associated with hematitic iron ore deposits, which likely formed through the interaction between cool, oxidizing sea water and the hot pillow basalts (Wedepohl *et al.* 1983; Von Raumer *et al.* 2017). These iron ore deposits roughly mark the boundary between the Givetian and Frasnian (379 Ma; Flick *et al.* 1990; Lippert & Flick 1998). Several minor thrusts cut through the ore deposits as a result of compression during the Variscan orogeny (Königshof *et al.* 2010). Phases of reduced volcanism allowed reefal limestone to form atoll-type features on top of the lavas. After the volcanic phase, debris flows and low density turbidites deposited debris composed of iron ore, reefal limestone and volcanic rocks in the area (Königshof *et al.* 2010).

The studied pillow lavas have not been severely affected by deformation (Nesbor 2007), and are thought to form a single coherent block, as no faults were observed in between the sampled pillows. Minor tilting and faulting occurred in the area during the Variscan orogeny. Some of the pillow lavas have a typical teardrop shape with the tip pointing downwards; this geopetal structure indicates a normal way-up position (Nesbor 2007). The pillows have an overall spilitic mineral assemblage (Flick *et al.* 1990), which is believed to be caused by diagenetic alteration right after the formation of the pillows. Chloritization has affected both the glassy rims of the pillows and the inside of the lavas, which gives a slight green colour to the rocks. Amygdules in the lavas are filled with chlorite towards the outside and filled with calcite towards the centre of the rocks (Nesbor 2007). Because of the alteration, the basalts are considered metabasalts. The reefs directly on top of the volcanics indicate that the pillow lavas were likely formed in a shallow marine environment. This environment is confirmed by the presence of several fossils such as calcimicrobes and stromatoporoids in the sediments surrounding the volcanics (Königshof *et al.* 2010; Königshof & Flick 2024).

Most mafic rocks in the Lahn-Dill area (Fig. 1b) are not suitable for zircon U-Pb geochronology due to their lack of zircons. Felsic rocks from this area yield an age range of 390–384 Ma, which can potentially be linked to Givetian volcanic activity in the Rheno-Hercynian Zone (Schulz-Isenbeck *et al.* 2019). The reef formation associated with the studied pillow lavas started in the middle Givetian (~383 Ma) according to conodont biostratigraphy, which indicates the Middle *varcus*-Subzone (Königshof *et al.* 2010; Franke *et al.* 2019; Königshof *et al.* 2024). The colour alteration index of the conodonts sampled in the sedimentary rocks surrounding the Philippstein section is 4.5–5, which represents a maximum heating temperature of 250–300 °C (Epstein *et al.* 1977; Rejebian *et al.* 1987). This is confirmed by Ahrendt *et al.* (1983) and Moe (2000) who describe a low degree metamorphism in the Rhenish Massif below closing temperatures of the K-Ar system (<350 °C). The temperatures in the sediments were likely reached because of the thermal energy resulting from the formation of the pillow basalts (Wedepohl *et al.* 1983; Von Raumer *et al.* 2017) and thus do not reflect a post-volcanism overprint. Only very low-grade metamorphism affected the research area during the Variscan orogeny (Moe 2000) and a low-grade regional metamorphic event occurred in the Lahn area between 340 and 330 Ma (Ahrendt *et al.* 1983).

After formation of the Middle Devonian volcanics and sediments of the Philippstein quarry, the depositional setting in the Rhenish Massif was dominated by mixed siliciclastic-carbonate systems and offshore basins where carbonates intercalate with basinal shales around the Frasnian-Famennian boundary (371.1 Ma). At the end of the Famennian stage (359.3 Ma), several sea-level changes occurred (e.g. Kaiser *et al.* 2016; Golonka 2020). The Early Mississippian (359.3–346.7 Ma) was characterized by increasing subsidence and extension of the continental crust on the southern shelf of Laurussia, accompanied by volcanic activity. The magmas of the lower Carboniferous cycle were almost entirely of tholeiitic composition (Nesbor 2019). The volcanic succession is followed by argillaceous sediments and/or limestone turbidites in the Visean stage (346.7–330.9 Ma) and later by flysch sediments. During the Variscan orogeny, Rhenohercynian nappes were thrusted over the autochthonous basement (Nesbor 2019). Gondwana and Laurussia

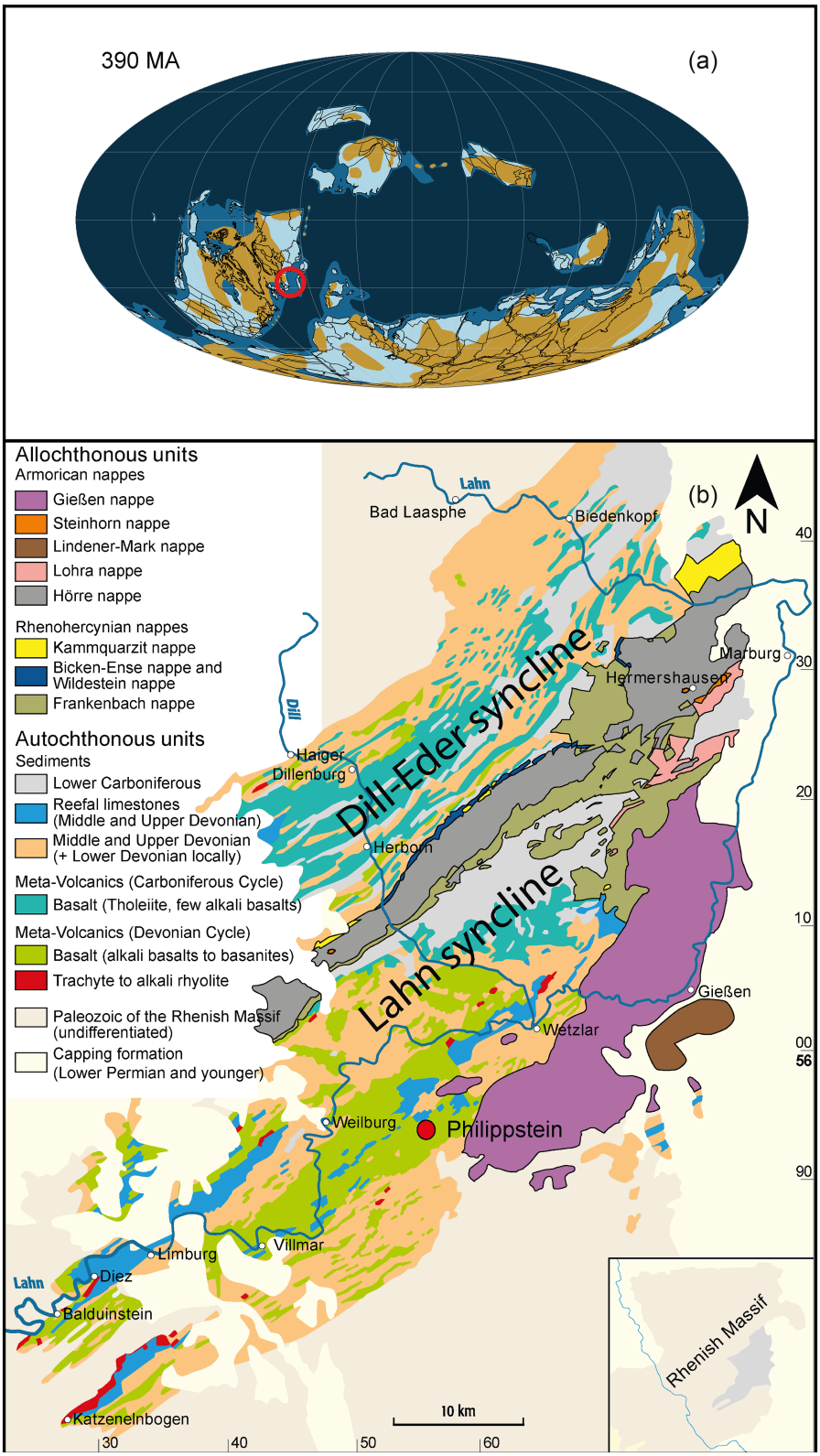

Figure 1. (a) Paleogeographic global map of the Middle Devonian after Marcilly *et al.* (2022). The red circle indicates the palaeoposition of the Rhenish Massif. Exposed land is indicated in beige, light blue colours indicate flooded continental shelves and dark blue indicates deep ocean. (b) Simplified geological map of the Lahn-Dill area in the Rhenish Massif. The location of the Devonian pillow lavas in the Philippstein quarry is indicated with the red circle (after Königshof *et al.* 2010).

collided, with large-scale faulting, metamorphism and magmatic intrusions as a result (Nesbor 2019).

3 METHODS

3.1 Sample selection and microscopic observations

In October 2021, we sampled fourteen pillow lavas in the Philippstein quarry in Braunfels, Germany. These pillows were collected within a ∼100-m range and form one unit. We therefore consider all samples to represent a single volcanic event. A minimum of eight cores was collected from every pillow, using a petrol-powered drill with a standard palaeomagnetic core diameter of 2.5 cm. The orientation of the drill cores was determined with a magnetic compass. A sun compass could not be used due to cloudy circumstances during sampling. No tilt correction was applied to the measured orientation, since the pillow lavas are in sub-horizontal position (Nesbor 2007).

The samples were processed in the palaeomagnetic laboratory Fort Hoofddijk at Utrecht University (the Netherlands). Petrographical and rock-magnetic properties of the samples were assessed to determine their suitability for a palaeomagnetic study. Palaeointensity and directional analyses were carried out in a magnetically shielded room with a maximum magnetic field of 400 nT. Additional analyses were carried out in the Iver Giæver palaeomagnetic laboratory of the University of Oslo (Norway).

Thin sections of all pillows were analysed with a Leica DM750 optical microscope in plane-polarized, cross-polarized and reflected light. Micrographs were produced with an attached DMC5400 digital camera. Secondary electron and backscattered electron images of carbon-coated thin sections were obtained using a Zeiss EVO15 Scanning Electron Microscope at the Electron Microscopy Centre of Utrecht University, with a 15 keV accelerating voltage, a 500-pA probe current and a 9.5–10 mm working distance. An Oxford Instruments Ultim-Extreme EDS detector was used to determine the elemental composition of the magnetic minerals present in the samples. Point measurements were acquired with a 15 keV accelerating voltage and a 1 nA probe current.

3.2 Rock-magnetic analyses

The anisotropy of magnetic susceptibility (AMS) was measured for 58 specimens selected from all pillow lavas using an AGICO MFK-1 Kappabridge with SAFYR7 software, applying a field of 200 A m^{-1} at a frequency of 976 Hz. Standard specimens with a 22 mm height were used and rotated through three orthogonal planes. The AMS parameters were calculated with the Anisoft5 software (AGICO).

The magnetic mineralogy of the samples was investigated by high-field thermomagnetic runs that were performed on one specimen per pillow lava, using a modified horizontal translation type Curie balance (Mullender *et al.* 1993). Eight series of heating and cooling were performed up to a temperature of 700 °C, with a cycling field of 150–300 mT. Susceptibility versus temperature curves up to 700 °C were acquired at the Iver Giæver laboratory of the University of Oslo. The runs were performed on powdered specimens of all pillows using an AGICO MFK1-FA Susceptometer and CS-4 furnace with a sensitivity of 10^{-8} SI. To estimate the magnetic grain size in the samples, hysteresis loops of both pillow bulk rock and pillow rims were measured using a Princeton Measurements Corporation MicroMag 2900 alternating gradient magnetometer (AGM). The loops were measured with a field ranging between −1.5 T and 1.5 T or −1.0 T and 1.0 T in field increments of 2 or 5 mT with an averaging time of 150 or 200 ms. The noise level of the MicroMag 2900 is 2×10^{-9} Am^2. The saturation magnetization (Ms), the saturation remanent magnetization (Mrs) and the coercive forces (Bc) of the samples were acquired after correction for the paramagnetic slope at 70 per cent of the field value using AGM software.

Acquisition curves of the isothermal remanent magnetization (IRM) were obtained with 43 field steps and a maximum applied field of 700 mT in a robotized 2G DC-SQUID magnetometer (Mullender *et al.* 2016). The analysis was carried out on 74 specimens selected from all sampled pillows. The data were processed using the MAX UnMix web application by Maxbauer *et al.* (2016).

3.3 Demagnetization experiments

Three different demagnetization techniques were applied to isolate the characteristic remanent magnetization (ChRM) in the samples: alternating field (AF) demagnetization, thermal demagnetization, and a combination of both techniques. Interpretation was done in the interpretation portal of paleomagnetism.org (Koymans *et al.* 2016; 2020) by analysing the decay curves and vector endpoint diagrams (Zijderveld 1967). Mean directions were calculated with the use of principal component analysis (Kirschvink 1980).

3.3.1 AF demagnetization

The AF demagnetizations were performed on 116 specimens, which equals eight specimens per pillow on average. Eighteen AF steps were applied, up to a maximum field of 270 mT with an automated sample handler and the measurements were conducted with the robotized 2G DC-SQUID magnetometer (Mullender *et al.* 2016). At least four consecutive demagnetization steps were used for ChRM interpretation, no anchoring was applied and a maximum angular deviation (MAD) cut-off of 10° was used.

3.3.2 Thermal demagnetization

Thermal demagnetization was carried out to isolate the ChRM as well as assess the suitability of the samples for palaeointensity measurements. The NRM of three to four specimens per pillow was stepwise thermally demagnetized, totalling 47 specimens. The measurements were carried out with a 2G DC-SQUID magnetometer, and the heating was performed in a magnetically shielded furnace based on the ASC TD-48SC thermal demagnetizer. Fourteen thermal steps were applied, up to a maximum of 630 °C. The unblocking temperature spectra from these measurements aid in determining the optimal temperature steps for palaeointensity experiments. The room temperature measurement is not included in the interpretation of the analyses to exclude low-temperature (viscous) overprints from the results. No anchoring was applied and no MAD cut-off was used. At least five consecutive demagnetization steps were used for the high-temperature data interpretation.

Great circle analysis was used when no ChRM decayed towards the origin, due to components with overlapping blocking temperatures or coercivities. Lines (ChRMs; set points) and planes (great circles) were determined using the eigenvector approach of Kirschvink (1980). We use the method of McFadden & McElhinny (1988) to determine great-circle solutions.

3.3.3 Combined AF and thermal demagnetization

A combination of AF and thermal demagnetization was performed at the Iver Giæver laboratory of the University of Oslo. Measurements of NRM were performed using a WSGI (2G) Model 755 Superconducting Rock Magnetometer. The samples were demagnetized using the LDA-5 automated, computer-controlled AF demagnetizer, following the protocol of Finn & Coe (2016). This protocol permutes the demagnetization axes to eliminate gyroremanent magnetizations (GRMs) in the directional calculations. Demagnetization of this set of samples was done with the permuted protocol up to 12 mT. Subsequently these samples were further thermally demagnetized with 22 temperature steps with increments ranging between 10 °C and 100 °C, up to a maximum temperature of 580 °C. This procedure is used to distinguish potential overprints from the potentially primary signal. The measurements were carried out on a total of 56 specimens, selected from all pillow lavas. No anchoring was applied and no MAD cut-off was used for the data interpretation. At least five consecutive demagnetization steps are used to determine the ChRM. The AF demagnetization steps below 12 mT are not included in the interpretation, in order to exclude low-coercivity components possibly influenced by viscous multidomain behaviour.

Besides the univectorial analysis, great-circle solutions were found in a similar fashion as described for thermal demagnetization.

3.4 Palaeointensity experiments

3.4.1 IZZI-Thellier

Nine to ten specimens per pillow lava were subjected to the IZZI-Thellier protocol (zero-field, in-field, in-field, zero-field, pTRM-check; based on Tauxe & Staudigel 2004 and Yu *et al.* 2004) to determine their absolute palaeointensity. Additionally, vitrified rims were present around three of the pillow lavas and five specimens per rim were subjected to thermal palaeointensity experiments. Specimens typically weigh 0.1–0.5 g to ensure that their magnetic moments do not exceed the dynamic range of the 2G DC-SQUID magnetometer and they are glued inside quartz-glass holders to facilitate sample mounting. A laboratory field of 10 μT was chosen, as this is an estimate of the strength of the Middle Devonian geomagnetic field (Bono *et al.* 2022b). The temperature steps used for the IZZI-Thellier palaeointensity experiments are based on the rock magnetic analyses and the thermal demagnetization behaviour of the pillow lavas. Heating of the specimens was done in a magnetically shielded furnace based on the ASC TD-48SC thermal demagnetizer, with in-house developed temperature control whereby temperature overshoots are lower than 2 °C. Part of the specimens start to unblock most of their NRM at relatively low temperatures (∼200 °C). For these specimens temperature increments of 40 °C were used within the temperature range 200–560 °C. Partial thermoremanent magnetization (pTRM) checks were done at 200, 240, 320, 400 and 480 °C. For the specimens with a higher unblocking temperature starting at ∼300 °C temperature increments of 30 °C were used within the temperature range 300–570 °C. The pTRM-checks for this set were done at 300, 330, 390, 450 and 510 °C. For the vitrified rims temperature increments of 35°C were used in a temperature range of 200–515 °C. The pTRM-checks were done at 200, 235, 305, 375 and 445 °C. The IZZI-Thellier results were interpreted using the paleointensity.org package (Béguin *et al.* 2020). The modified selection criteria as defined in Paterson *et al.* (2014) and Cromwell *et al.* (2015) were used to derive an absolute palaeointensity from the data.

3.4.2 Full laboratory TRM as indicator of NRM recording

To assess the palaeomagnetic recording fidelity of samples with a weak NRM, a full TRM was applied to a selection of thermally stable samples. Based on thermomagnetic and susceptibility versus temperature data, ten samples were selected for this test. From each of these samples, five sister specimens were created. These were first fully thermally demagnetized at a maximum temperature of 615 °C. In a second thermal cycle, they were given a TRM in several laboratory fields (TRM1). Each specimen was subjected to one thermal cycle to make the TRM data comparable and avoid continuing thermal alteration. The TRM field values of 2, 5, 10, 15 and 30 μT were imparted by cooling from 615 °C to room temperature. These field values were selected because they are in line with expectations for the Devonian magnetic field. To ensure the reproducibility of the results, a second full TRM (TRM2) was imparted and measured as well. In between all steps the samples' susceptibility was measured with an AGICO MFK-1 Kappabridge, at a field intensity of 200 A m^{-1} and an operating frequency of 976 Hz. All samples with a change in susceptibility > 20 per cent between the NRM state and the fully demagnetized state are omitted from the results. All samples with a change in susceptibility > 10 per cent between TRM1 and TRM2 are also omitted from the results. Both these choices were made to exclude samples with major alteration. Furthermore, samples with an intensity difference of > 20 per cent between TRM1 and TRM2 are also omitted.

4 RESULTS

4.1 Petrography

The pillow basalts consist of a fine-grained groundmass and three pillows contain vitrified rims of < 2 cm thickness. It should be noted that the rims have an aphanitic texture with some vitrification, rather than a glassy texture. Representative micrographs of the samples in plane polarized light (PPL) and SEM images of the samples are shown in Fig. 2. All samples have a typical fine-grained, homogenous (meta-)basaltic composition. The groundmass consists of relatively equant crystals. The mineral assemblage of the metabasalt consists of plagioclase and (chloritized) clinopyroxene with a subophitic texture; some larger clinopyroxene phenocrysts of < 0.3 mm are present. The modal percentages of the minerals are 50–60 per cent plagioclase, 35–45 per cent clinopyroxene and 5 per cent opaque minerals. The plagioclase is typically elongated and < 0.1 mm in size. The clinopyroxene in the groundmass is anhedral and < 0.1 mm in size. The opaque minerals range in size from submicron to tens of microns and mainly consist of (titano-)magnetite, as determined from Energy-Dispersive X-ray Spectroscopy (EDS) analysis. The magnetite is typically sub- to euhedral cubic in shape, but some small skeletal magnetite is present as well. The rocks are affected by chloritization through metasomatism, which is present throughout the sample and gives the rocks a slightly green appearance, although the original basaltic texture is still present. The chloritization is an alteration product associated with the cooling of the pillow basalts in sea water (Wedepohl *et al.* 1983; Von Raumer *et al.* 2017). Few small, subparallel calcite veins cut through the pillows and contain acicular magnetite. Vesicles in

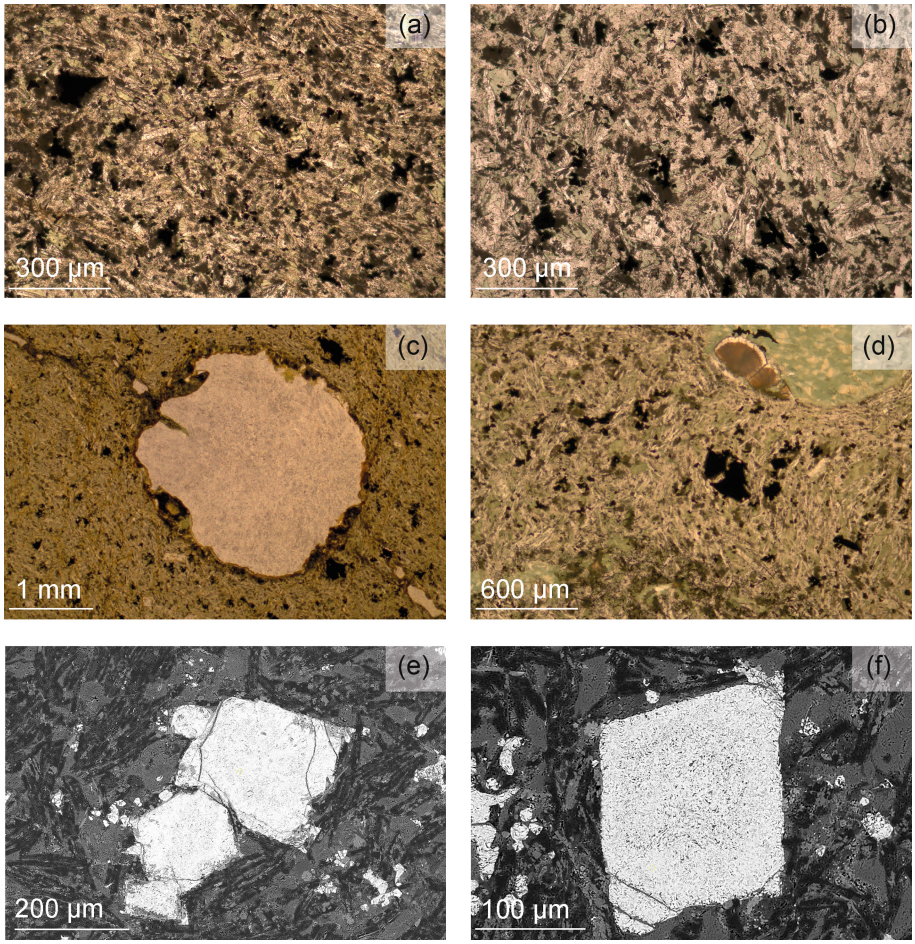

Figure 2. (a)–(b) Micrographs of representative samples in plane polarized light with 100x magnification. The samples are fine-grained (meta-)basalts with chloritization present throughout. The groundmass consists of plagioclase and pyroxene and is specked with black iron oxides. (c) Micrograph of a vesicle filled with calcite. (d) Micrograph of extensive (green) chloritization of the (meta-)basalt. (e)–(f) SEM photographs of representative samples. The main shape of magnetite is sub- to euhedral cubic and the size varies from submicron to tens of microns in diameter.

the interior of the pillow basalts are filled with calcite and sometimes amygdules with chlorite are present close to the rims of the pillows.

Fe-Ti oxides are present throughout the samples between plagioclase and clinopyroxene crystals as determined by EDS. Exsolved ilmenite lamellae hardly occur, which corresponds to an oxidation index of I-II of Watkins & Haggerty (1967). This equals a deuteric alteration with a maximum Fe_2O_3:FeO of approximately 0.8. The titanium amount in the magnetite varies strongly, the typical value is 3–5 wt per cent (TM15-TM25) but values up to >>9 wt per cent titanium are observed. Minor iron sulphides are observed as well.

4.2 Rock-magnetism

The pillow lavas cooled quickly, indicated by the presence of vitrified rims around some of them, and are hence considered instantaneous recorders of the magnetic field. The cooling rate is associated with the formation of small iron oxides, which are stable and reliable magnetic recorders, making them ideally suited for palaeomagnetic analysis. Several rock-magnetic tests were carried out to understand the nature and behaviour of the magnetic carriers in the pillow lavas. The rock-magnetic behaviour is similar in all fourteen pillows.

Curie balance measurements (Figs 3a–d) show an initial magnetization intensity of the samples varying from 1.51 to 3.71 $Am^2\,kg^{-1}$, indicating the presence of at least 1.5–4 per cent magnetite in the pillows. The M-T curves are characterized by a reversible decrease in magnetization until 350–400 °C. Above this temperature, the curves become increasingly less reversible, indicating that Thellier palaeointensity experiments will probably not be interpretable above 350–400 °C because pTRM checks will start failing due to mineral alteration. A steep decrease in magnetization occurs between 530 and 580 °C indicating that (Ti-)magnetite is the main magnetic carrier present in the rocks, which could be of primary origin and therefore hold a primary TRM. The sample in Fig. 3(c) has a small tail above 600 °C, which suggests a minor presence of maghemite. No hematite is expected in the samples, based on both the M–T curves and optical microscopy. The final cooling curve from 700 °C has a lower magnetization than the corresponding heating curve, likely due to the oxidation of (titano-)magnetite, which produces a less magnetic phase.

Magnetic susceptibility versus temperature curves (Figs 3e–h) indicate a clear magnetite presence and minor to medium alteration of the magnetic carriers above 350–400 °C, which corresponds to the observations of the M-T curves. All four samples show a small Hopkinson peak in the heating curves. Samples that experience the

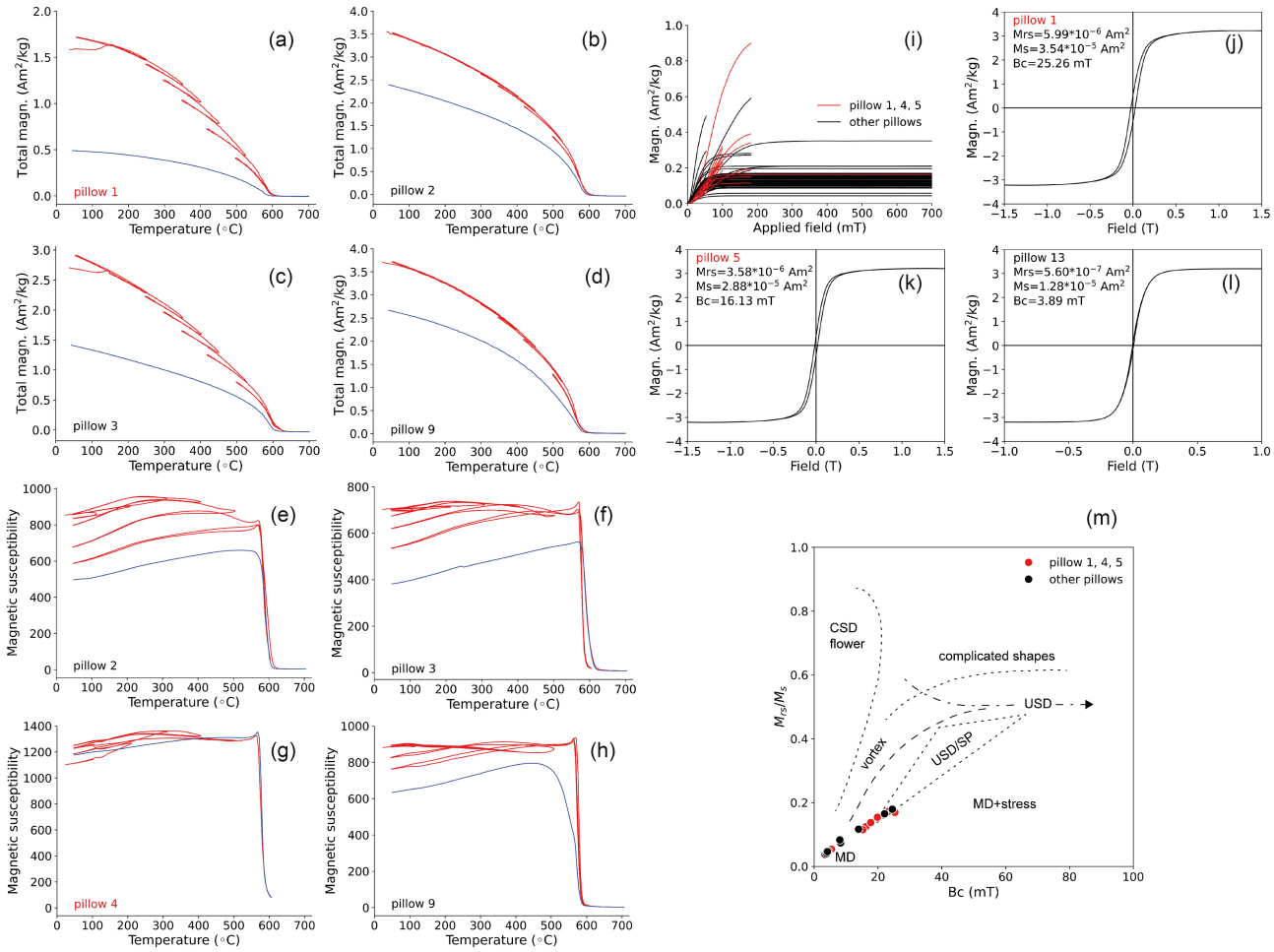

Figure 3. Analyses of samples from pillows 1, 4 and 5 are indicated in red, other pillows are indicated in black. The demagnetization behaviour of these two groups of pillows is somewhat different (Fig. 5). Further explanation is provided in the main text. (a)–(d) M-T analysis of representative samples from four different pillows. Heating curves are indicated in red, cooling curves in blue. All samples have typical magnetite Curie temperatures. Additionally, the slight tail above 580 °C in pillow 1 indicates minor maghemite. (e)–(h) Representative susceptibility versus temperature runs of samples from four different pillows. Heating curves are indicated in red, final cooling curves in blue. The samples show a typical magnetite signature and minor to medium alteration during heating above 350–400 °C. (i) IRM acquisition curves show that the main magnetic carrier in the samples is (Ti-)magnetite. Due to measurement problems, not all curves were measured up to 700 mT. (j)–(l) Representative slope-corrected hysteresis loops show low coercivities of the magnetic carriers. (m) The squareness versus coercivity plot based on Tauxe *et al.* (2002) reveals mainly multidomain behaviour. Part of the data points plot on the boundary of multidomain (MD) and uniaxial single domain (USD) particles. CSD indicates cubic single domain and SP indicates superparamagnetic grains in this plot.

least alteration (Figs 3g and h) are expected to behave most ideally during palaeointensity experiments.

IRM acquisition curves (Fig. 3i) show that most samples are fully saturated above 100 mT, indicating magnetite presence. Some samples are only fully saturated above 200 mT, which is probably caused by a higher Ti-content in the magnetite. Unmixing of the curves with the method of Maxbauer *et al.* (2016) revealed only one dominant magnetite population along with mathematical artefacts, providing no new insights into the magnetic mineralogy populations. Therefore, the results are presented in Fig. B1, Appendix B.

The Bc-values derived from the hysteresis loops (Figs 3j,k,l) are generally low, 3.4–25.3 mT, which indicates a weak capability of the samples to withstand an external magnetic field. M_{rs}-values range from 0.03 to 0.54 $Am^2\,kg^{-1}$ and M_s-values range from 0.71 to 4.94 $Am^2\,kg^{-1}$, indicating at least 1–7 per cent ferrimagnetic mineral presence in the samples. The magnetic moment is hardly increasing above 180 mT, which suggests that little high-coercivity minerals are present in the samples. Results from all Curie balance measurements, susceptibility versus temperature measurements and hysteresis loops are shown in Figs D1, D2, D3, Appendix D.

The squareness (magnetization ratio) versus coercivity plot (Tauxe *et al.* 2002) of the hysteresis results (Fig. 3m) clearly indicates multidomain (MD) behaviour and a mixed magnetic grain size. The MD behaviour might cause the low coercivities observed in the hysteresis loops, since it suppresses the coercivity signal of the smaller magnetic grains. The M_{rs}/M_s ratio varies between 0.04 and 0.17. The lower values suggest MD behaviour and therefore Thellier-style palaeointensity experiments are not expected to succeed. The higher values indicate pseudo-single domain (PSD) behaviour for at least part of the grains which could lead to successful palaeointensity results.

4.3 Anisotropy of magnetic susceptibility

The volume-normalized mean susceptibilities (Kmean) of the samples vary within the pillows, but most range between 3×10^{-2} and

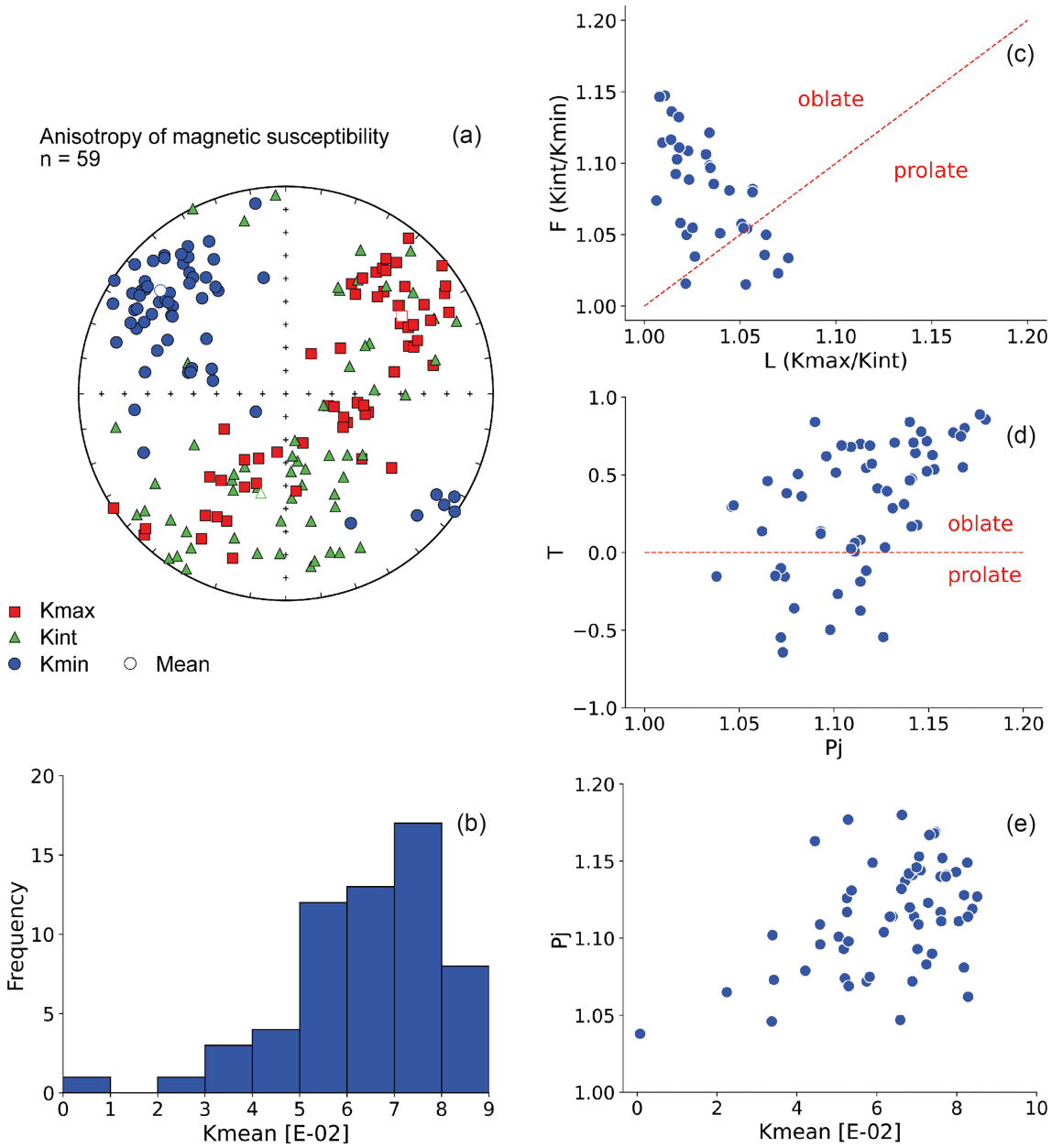

Figure 4. (a) Stereoplot with the three AMS directions collected from all pillow lavas. Kmin (mean 310°/24°) directions tend to cluster. The Kint (mean 057°/34°) and Kmax (mean 193°/47°) distributions are overlapping and form a girdle. (b) Frequency of mean susceptibility (Kmean), the values are generally high and indicative of ferrimagnetic mineral presence. (c) Lineation (Kmax/Kint) versus foliation (Kint/Kmin) indicate a dominantly oblate magnetic fabric. (d) Jelinek plot with corrected anisotropy degree (Pj) versus shape factor (T) indicates that the dominantly oblate magnetic fabric is not clearly related to the anisotropy degree. (e) The mean susceptibility (Kmean) versus corrected anisotropy degree (Pj) show no linear relationship.

9×10^{-2}, with a median value around 7×10^{-2} to 8×10^{-2} (Fig. 4b). These values are typical for a susceptibility dominated by ferromagnetic minerals. Therefore, the anisotropy of magnetic susceptibility (AMS) reveals the fabric of ferromagnetic minerals. AMS measurements of the pillow lavas (Fig. 4) show that they are mainly magnetically foliated and that they are characterized by a variable degree of anisotropy, reaching from a low degree of anisotropy (Pj) of 1.04 to high values of 1.18 with a mean value of 1.12. The foliation (F) exhibits a wide range of values from 1.01 to 1.15 and a mean value of 1.08. The lineation (L) shows a smaller range and varies from 1.01 to 1.09 with a mean value of 1.03. The mean equals the median for all three parameters. Since Fmean is higher than Lmean, the AMS ellipsoids are mainly oblate (Fig. 4c). No clear correlation is present between the AMS ellipsoid shape (T) and the anisotropy degree (Fig. 4d), except that the highest Pj values correspond to an oblate character. There is no linear relationship between Pj and Kmean (Fig. 4e), indicating that no correlation between the amount of magnetic minerals and the mineral arrangement is present. In other words, the variation in Pj is not caused by petrographic variations. Therefore, the AMS values can be interpreted as structural indicators (Fig. 4a). The mean direction of Kmax is dec = 193°, inc = 47° and the mean direction of Kint is dec = 057°, inc = 34°. The directions of Kmax and Kint are scattered in a practically overlapping girdle, with overlapping confidence circles. The mean direction of Kmin is more clustered and has values of dec = 310°, inc = 24°. The higher Pj values may suggest that the rocks have

been deformed after their formation and contain a preferred magnetic direction due to a compressional tectonic regime. The regional tectonic structures in the study area are NE-SW trending as a result of the Variscan orogeny (Moe 2000; Königshof *et al.* 2010), which roughly corresponds to the Kmin direction. However, the Pj values differ strongly within each pillow with no obvious relationship related to their location within the pillow nor to the core-rim distance (Table 1). A varying chlorite content in the samples, with microcrystalline magnetite inclusions, could explain a high variation in Pj throughout the pillows. A low Pj is usually considered as a magmatic fabric; however, the Pj distribution is random per pillow which makes a magmatic fabric unlikely. Other values of the abovementioned AMS parameters per pillow also do not reveal clear trends. Only the shape factor of the samples from the pillow rims is higher than the shape factor of the pillow core samples. This indicates that more oblate shapes are present in the rims than in the cores.

4.4 Palaeomagnetic directions

We sampled fourteen pillow lavas within a continuous block of ∼100 m width. While we cannot certainly exclude any tilting that happened after formation of the pillows, we consider the presence of vertical columnar joints at the top of the block and the downwards pointing geopetal structure of some pillows as an indication that the pillows have likely not been tilted significantly. Therefore, no tectonic correction is required on the obtained palaeomagnetic directions. We did not observe faults or other structures in between the pillows, and the pillows show no indications that they have moved relative to each other. All pillows are considered to be part of the same volcanic event because of the absence of sedimentary infilling between the pillow basalts, therefore, no temporal difference is assumed.

4.4.1 Demagnetization behaviour

The demagnetization behaviour observed in three different experiments, AF, thermal and a combination of AF and thermal demagnetization, is shown in Fig. 5. The starting NRM intensity ranges between 6.31×10^{4} and 7.55×10^{6} μA m^{-1}. Examples of representative Zijderveld diagrams (Figs 5a, b, d, e, g, h) indicate the differences in data quality between the different experiments. Samples that were subjected to AF demagnetization show univectorial behaviour and demagnetize towards the origin, sometimes surpassing it at high AF values of >100 mT. Most thermally demagnetized samples show less straightforward behaviour, often with multiple components that do not demagnetize to the origin but show rather curved paths of demagnetization.

The median destructive field of AF demagnetization lies around 10 mT (Fig. 5c). Most samples lose their magnetization rapidly between 0–15 mT and more gradually at higher fields. Samples that deviate from this typical demagnetization behaviour are indicated in red, these outliers are samples from pillows 1, 4 and 5. Low coercivity components are generally interpreted up to 15 mT, high coercivity components are interpreted from 15 mT up to a maximum of 100 mT. Thermal demagnetization is generally gradual in most samples, with a typical median destructive temperature above 200–250 °C (Fig. 5f). Low-temperature components are generally interpreted up to 250 °C, high-temperature components are interpreted from 250 to 500 °C up to a maximum of 630 °C. The same three pillows indicated in red in Fig. 5(c) also show deviating thermal demagnetization behaviour, with rapid demagnetization

Table 1. AMS parameters per pillow, further defined based on distance to edge of pillow. Rim values indicate values of all measurements < 15 cm from the edge of the pillow. Core values indicate values of all measurements >15 cm from the edge of the pillow. Note that these distances were determined on the 2D plane of the outcropping pillow, it can therefore only be considered as a rough estimate of the actual distance from the rim in 3D space. Most values are random and do not indicate any correlations. Only the T(rim) is higher on average than T(core). This indicates that more oblate shapes are present in the rims of the pillows compared to the pillow cores.

pillow	mean Kmax	mean Kint	mean Kmin	mean Pj	Pj(core)	Pj(rim)	mean F	F(core)	F(rim)	mean L	L(core)	L(rim)	mean T	T(core)	T(rim)
1	–	–	–	–	–	–	–	–	–	–	–	–	–	–	–
2	224/18	105/57	324/27	1.150	1.137	1.156	1.111	1.086	1.124	1.026	1.044	1.017	0.601	0.312	0.745
3	199/50	063/31	318/23	1.105	1.105	–	1.046	1.046	–	1.056	1.056	–	−0.102	−0.102	–
4	035/38	218/52	127/02	1.077	1.083	1.046	1.043	1.045	1.029	1.030	1.033	1.016	0.148	0.119	0.295
5	054/34	194/50	310/21	1.112	1.109	1.115	1.087	1.084	1.089	1.015	1.016	1.015	0.690	0.680	0.699
6	040/32	175/49	294/23	1.119	1.112	1.133	1.080	1.077	1.087	1.031	1.027	1.038	0.397	0.417	0.355
7	109/66	215/08	307/23	1.092	1.103	1.047	1.044	1.047	1.030	1.044	1.051	1.016	0.032	−0.036	0.304
8	047/24	185/60	308/18	1.154	1.177	1.150	1.120	1.146	1.116	1.019	1.008	1.020	0.695	0.889	0.663
9	213/31	075/51	316/22	1.100	1.078	1.111	1.064	1.035	1.078	1.030	1.039	1.025	0.281	−0.092	0.468
10	082/47	203/26	310/33	1.126	1.122	1.142	1.087	1.081	1.111	1.031	1.034	1.018	0.477	0.419	0.708
11	134/46	238/14	340/41	1.141	1.142	1.140	1.097	1.080	1.115	1.033	1.056	1.009	0.504	0.168	0.841
12	101/59	225/20	324/24	1.100	1.111	1.090	1.064	1.054	1.074	1.030	1.054	1.006	0.424	0.007	0.841
13	205/44	046/43	305/11	1.135	1.130	1.149	1.090	1.084	1.106	1.036	1.038	1.032	0.395	0.352	0.524
14	070/27	166/26	292/52	1.110	–	1.110	1.050	–	1.050	1.055	–	1.055	−0.066	–	−0.066

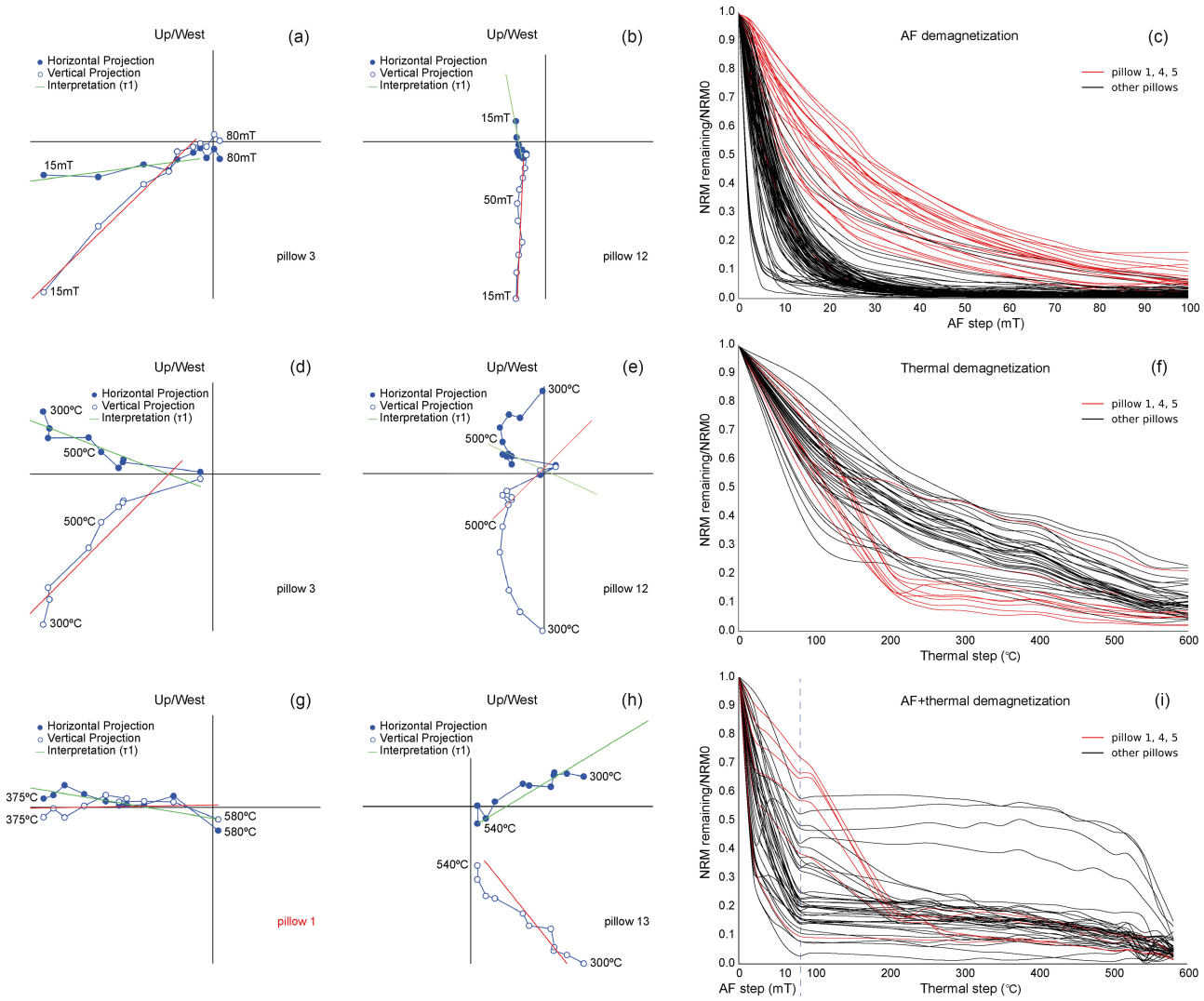

Figure 5. (a)–(b) Typical Zijderveld diagrams of AF demagnetization, (d)–(e) thermal demagnetization and (g)–(h) AF + thermal demagnetization experiments. Two representative samples in geographic coordinates are plotted for each demagnetization method. (c) The median destructive field of AF demagnetization has a value of approximately 10 mT for most samples. (f) The thermal demagnetization rate is gradual above 100 °C for most samples. (i) Demagnetization behaviour of the combination of AF demagnetization (0–12 mT) and thermal demagnetization (100–580 °C). Samples indicated in red in (c) and (f) demagnetize differently than the bulk of the samples. Data from these pillow lavas are indicated in red in all rock-magnetic plots (Fig. 3) and equal area plots (Fig. 6).

until 200–250 °C and then slow demagnetization until 500–600 °C (Fig. 5f). The mean directions from these three pillows are indicated in red on all equal area plots of Fig. 6. No obvious explanation for this difference in demagnetization behaviour is suggested by the rock-magnetic results (Fig. 3).

4.4.2 Directional analysis

The characteristic remanent magnetizations (ChRMs) from AF demagnetization, thermal demagnetization and a combination of both, are scattered and indicate ambiguous results, which are summarized in Table 2. Devonian magnetizations typically show overprints acquired during the Kiaman reverse superchron (e.g. van der Boon *et al.* 2022 and references therein). The apparent polar wander path of Torsvik *et al.* (2012) predicts a reverse polarity direction for the study area of dec ≈ 207° and inc ≈ 11° at the beginning of the Kiaman (∼320 Ma) and a normal polarity direction of dec ≈ 202° and inc≈−35° at the end of the Kiaman (∼260 Ma). A present-day magnetic overprint is also regularly present in Devonian rocks (e.g. van der Boon *et al.* 2022 and references therein), which would correspond to a direction of dec ≈ 0° and inc ≈ 66° in the study area. The palaeoposition of Germany during the Middle Devonian indicated in Fig. 1 is 20°–25° south of the equator, this would lead to inclinations of 36°–43° in a dipolar geomagnetic field. Zwing & Bachtadse (2000) found a reverse direction of dec = 198°, inc = 40° for the Late Devonian in southwestern Germany.

The results of the AF demagnetization experiments are shown in Figs 6(a)–(c). At coercivities below 15 mT (Fig. 6a) the results are scattered and the mean value of dec = 166°, inc = 85° does not correspond to an expected Devonian inclination, nor to a Kiaman or present-day field direction. The samples seem to be influenced by viscous multidomain behaviour, which we observed from the lack of reproducibility of NRM measurements when samples were kept in a shielded lab environment for several weeks. For the interpreted coercivities above 15 mT (Fig. 6b) a large spread in negative

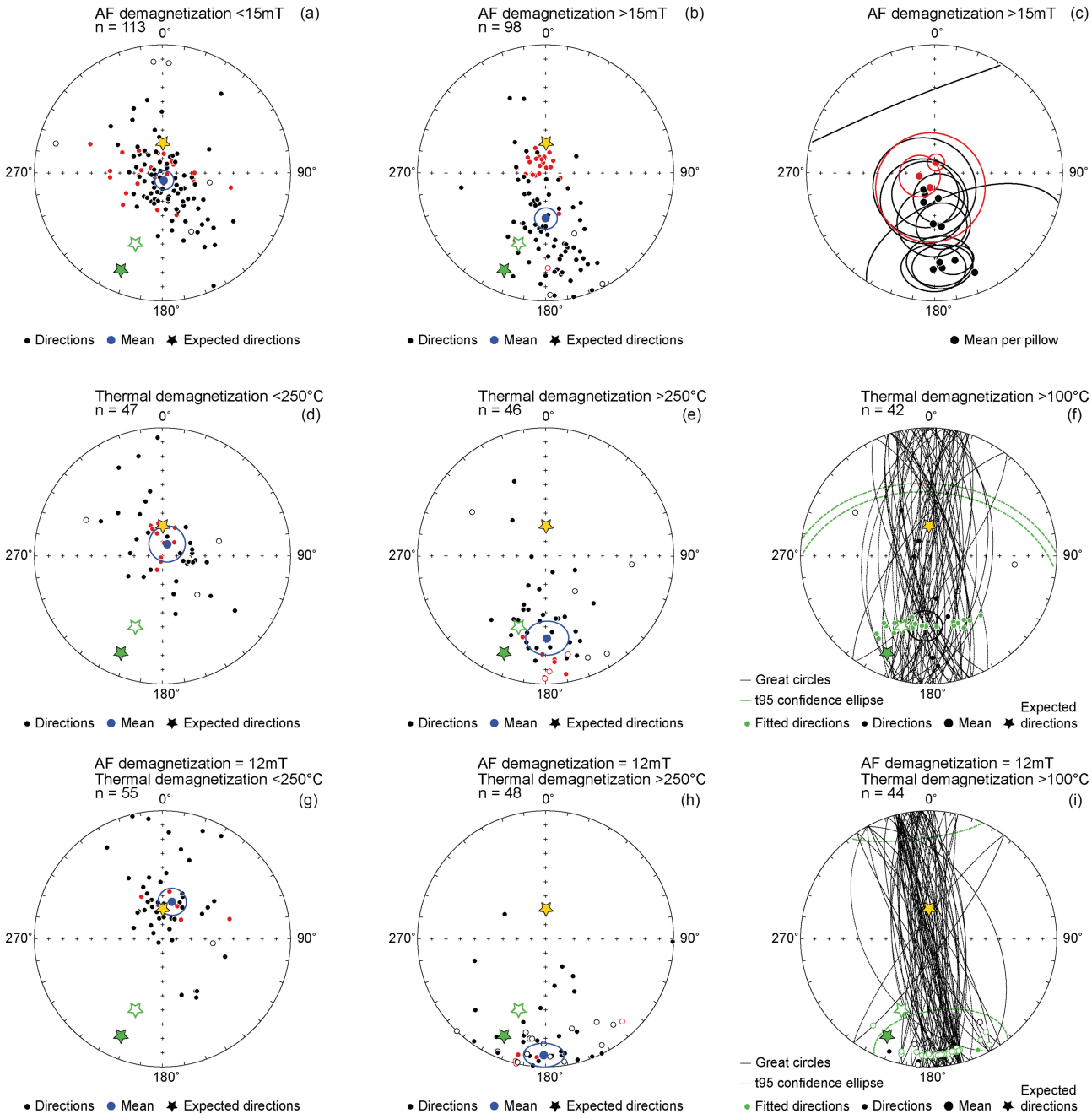

Figure 6. (a)–(c) Equal area plots of interpreted directions from AF demagnetization, (d)–(f) thermal demagnetization and (g)–(i) AF + thermal demagnetization analysis of the fourteen pillow lavas. Open circles and stars represent positive inclinations, closed circles and stars represent negative inclinations. The stars indicate potential overprints based on the Eurasian APWP by Torsvik *et al.* (2012), the green closed star represents the Carboniferous (320 Ma) expected direction, the green open star represents the Permian (260 Ma) expected direction and the yellow star represents the present-day field direction (IGRF; Alken *et al.* 2021). Analyses of samples from pillows 1, 4 and 5 are indicated in red in the equal area plots, other pillows are indicated in black. The demagnetization behaviour of these two groups of pillows is somewhat different. Further explanation is provided in the main text. The resulting palaeomagnetic directions are scattered but result in a mean declination and mean inclination of (a) dec = 166°, inc = 85°, with $\alpha_{95} = 5.98$ for low coercivity AF demagnetization; (b) dec = 180°, inc = 61°, with $\alpha_{95} = 6.92$ for high coercivity AF demagnetization; (c) The mean high coercivity directions per pillow are indicated in; (d) dec = 022°, inc = 82°, with $\alpha_{95} = 11.40$ for LT demagnetization; (e) dec = 179°, inc = 36°, with $\alpha_{95} = 12.10$ for HT demagnetization; (g) dec = 015°, inc = 65°, with $\alpha_{95} = 8.74$ for LT demagnetization after AF demagnetization up to 12 mT; (h) and dec = 181°, inc = 10°, with $\alpha_{95} = 9.8$ for HT demagnetization after AF demagnetization up to 12 mT. From great circle analyses a mean declination and inclination from the thermal demagnetization experiments is determined at (f) dec = 183°, inc = 44°, with $\alpha_{95} = 10.38$; (i) the AF + thermal demagnetization experiments result in dec = 173°, inc = −10°, with $\alpha_{95} = 3.67$.

inclinations is found (0°–89°) and the directions show a smeared distribution, which is not easily explained by overprinting. This smearing is also evident when the means per pillow are plotted (Fig. 6c). The grand mean of these data is dec = 180°, inc = 61°. The simultaneous demagnetization of two components can result in such a distribution, however no two components were identified. The Zijderveld diagrams show univectorial behaviour, which is atypical when two magnetic components are present. Viscous multidomain

Table 2. Tabulated expected declinations and inclinations and results from this study.

Expected results	Present-day field	Kiaman 260 Ma	Kiaman 320 Ma	Middle Devonian				
Declination	000°	202°	207°	198[a]				
Inclination	66°	−35°	11°	40°[a]/43°[b]				
Results	**Low coercivity**	**High coercivity**	**Low**	**High**	**Great circles**	**AF + low**	**AF + high**	**Great circles**
n/N	**AF**	**AF**	**temperature**	**temperature**	**(thermal)**	**temperature**	**temperature**	**(AF + thermal)**
	113/116	**98/116**	**47/47**	**46/47**	**42/47**	**55/56**	**48/56**	**44/56**
Declination	166°	180°	22°	179°	183°	15°	181°	173°
Inclination	85°	61°	82°	36°	44°	65°	10°	−10°

[a]Based on the directions from Zwing & Bachtadse (2000).
[b]Based on the palaeoposition of the study area from Marcilly *et al.* (2022).

behaviour is unlikely to be the cause of the smeared distribution, since this should have been removed by the 15 mT demagnetization. The presence of a GRM could be another explanation, although this is only clearly observed for the highest AF levels (>100 mT) that are not considered here (Fig. A1, Appendix A). When looking at the results in specimen coordinates, they do not plot perpendicular to a specific demagnetization axis (Fig. A2, Appendix A), excluding an obvious influence of the AF demagnetization protocol.

The thermal demagnetization results are shown in Figs 6(d)–(f). At temperatures below 250 °C (Fig. 6d) the results are scattered but have a mean of dec = 022°, inc = 82°, which roughly corresponds with a present-day field direction. The high-temperature demagnetization components (Fig. 6e) are scattered and have a mean of dec = 178°, inc = 36°. This result is somewhat similar to the result of the high coercivity AF components. This does not correspond to a present-day overprint, nor a Kiaman overprint. The inclination is close to the expected inclination based on the palaeoposition of the study area, so it could tentatively be a Devonian direction. However, another potential explanation was found with great circle analysis of the thermal demagnetization data (Fig. 6f). The ChRMs for many of the thermal demagnetization data describe paths along great circles from declinations around ∼0° towards ∼180°. The resulting fitted directions using the ChRM set points from thermal demagnetization experiments (Fig. 6f) have a mean declination and inclination of dec = 183°, inc = 44°. This does not correspond to the Kiaman nor the present-day field direction. However it falls on a plane that combines these two overprint directions, this suggests that a combination of a present-day overprint and Kiaman overprint could lead to the observed mean direction.

The results in Figs 6(g)–(i) were obtained after a demagnetization of 12 mT was carried out, to remove MD behaviour and thereby improve thermal demagnetization results. Here, the low-temperature component yields a mean of dec = 015°, inc = 65°. Although the results are scattered, this is potentially a present-day overprint. For the high-temperature component, an overall mean of dec = 181°, inc = 10° was found. This could potentially be interpreted as a Devonian direction. However, the ChRMs for many of the AF + thermal demagnetization data describe paths along great circles from declinations around 350° towards 170° (Fig. 6i) in a narrower manner than for thermal demagnetization alone (Fig. 6f). Great circle analysis results in a fitted mean direction of dec = 173°, inc = −10°. Although the declination deviates approximately 30° from the expected value for the Kiaman, the reversed inclination could agree with a Kiaman reversed component acquired between 320 and 260 Ma. Local tectonic rotations are not well known for the study area but could explain the observed declination. If no rotation occurred, the great circles could potentially be the combined result of a present-day overprint and a Devonian direction.

Summarizing, although the data scatter is high in all analyses, few interpretations seem possible. A present-day field overprint could possibly be interpreted from both low-temperature demagnetization experiments and from great circle analysis (Figs 6d, f, g, i). The influence of a Kiaman overprint may be inferred from great circle analysis of the thermal experiments (Fig. 6f) or from the AF + thermal experiments if a tectonic rotation is involved (Fig. 6i). Since the quality of the AF + thermal demagnetization data is expected to be the highest, the high-temperature analysis of these experiments is considered most trustworthy. These results could very tentatively be interpreted as Devonian, as the directions do not match a present-day field nor Kiaman overprint. However, the data quality is poor and the inclination of 10° is lower than expected for the palaeoposition

of the study area. In all cases, it is evident that no clear Devonian direction nor a Kiaman overprint can be easily distinguished in the samples, as the only way to resolve a possible Kiaman component is by using great circle analysis.

Three pillows show demagnetization behaviour different from the other pillows (Fig. 5c), these three pillows are indicated in red in Fig. 6 as well. The directions determined from these three pillows have similar directional means with high inclinations at high coercivities (Figs 6b and c). In the thermal demagnetization experiments, the directional clustering is less pronounced. Although these three pillows stand out in both demagnetization behaviour and directions, no clear explanation was found to explain this. We make no further assumptions about the quality of the directional data per pillow, based on these results.

4.5 Palaeointensity

4.5.1 IZZI-Thellier

Thermomagnetic curves of all pillow lavas indicate magnetite as a potential primary magnetic recorder and show reversible behaviour until 350–400 °C (Figs 3a–d). Susceptibility versus temperature experiments show minor to medium alteration above these temperatures (Figs 3e–h). Therefore, the pillow lavas would be promising targets for thermal palaeointensity experiments, although pTRM checks might not always be successful for temperatures exceeding 350–400 °C due to thermochemical alterations.

Thellier type experiments (Thellier & Thellier 1959) carried out with the IZZI-protocol (based on Tauxe & Staudigel 2004; Yu *et al.* 2004) consistently show non-ideal behaviour and generally do not pass selection criteria. Strong zig-zagging and high β-values suggest MD behaviour in most experiments. Only 7 per cent of the specimens pass the β-value criterion of ≤ 0.15. Of the pTRM checks, 16 per cent pass the DRAT-value ≤ 10 and 30 per cent pass the CDRAT-value ≤ 11, indicating that mineral alterations during heating occurred. The majority of the pTRM-checks do not return to the corresponding NRM data points indicating non-ideal behaviour from multidomain magnetite grains (Yu & Dunlop 2003). Only five specimens out of 127 passed the modified selection criteria as defined in Paterson *et al.* (2014) or Cromwell *et al.* (2015) using the interpretation portal of paleointensity.org (Béguin *et al.* 2020). Of these five palaeointensities, only one is accepted. This success rate of < 2 per cent is unusually low, while normally success rates of 10–20 per cent are achieved for absolute paleointensity determinations (Valet 2003).

From the three successful bulk rock results, only the palaeointensity estimate of 5.9 μT determined for pillow 11 is accepted (Fig. 7a). This palaeointensity is determined in the temperature range 200–520 °C and passes the selection criteria sets of TTB and SELCRIT2. The vitrified rim of pillow 8 (Fig. 7d) yields interpretable results in the temperature range 200–515 °C and indicates a field strength of 21.5 μT. However, the linear regression is of low quality, the results show strong zig-zagging behaviour and have a high β-value > 1, it is therefore not accepted. This sample passes the selection criteria of TTB, however, the pronounced MD behaviour makes the result unreliable.

Fits from two other bulk samples (Figs 7b and c) and another vitrified rim sample (Fig. 7e) pass some sets of selection criteria but include the room temperature step. Measurements below the temperature needed to remove any overprint cannot be accurately interpreted and are therefore rejected. Furthermore, the pTRM checks do not return to the corresponding NRM data points in Figs 7(c) and (e), indicating the low quality of the results.

The reliability of the palaeointensity results was assessed by using the Q_{PI}-criteria as defined by Biggin & Paterson (2014) and Bono *et al.* (2022a). The QAGE, QTRM, QALT, QACN and QMAG criteria are met, resulting in a Q_{PI}-value of 5 for the pillow lavas.

4.5.2 Full laboratory TRM as indicator of NRM recording

How the pillow basalts respond to an imparted TRM is shown in Fig. 8. The results are filtered based on differences in susceptibility and intensity, as outlined in Chapter 3.4.2, leaving 15 of 50 measurements for consideration. Generally, TRMs imparted in higher fields are larger (Figs 8a and b) as expected from theory (e.g. Dunlop & Özdemir 1997).

When comparing the imparted TRM to the NRM of the specimens (Figs 8c and d), a decreasing trend is observed. If the NRM of the pillow basalts represents a primary TRM, the ratio between the NRM and the laboratory TRM would be expected to approach 1 at a field intensity similar to that present during their formation, in line with the idea behind multispecimen palaeointensity procedures (Dekkers & Böhnel 2006; Fabian & Leonhardt 2010). The NRM/TRM ratio is closest to 1 for an imparted TRM of 2–5 μT, suggesting that the geomagnetic field at the time of the formation was close to that value. This interpretation aligns with the obtained palaeointensity result (Fig. 7a).

However, if the NRM of the specimens resulted from another mechanism than TRM, we would expect the ratio to be lower than 1, as other mechanisms are less efficient in imparting magnetizations compared to TRM. Hence, we deem the obtained results supportive of a low field at the time of pillow formation, but we do not consider it solid proof.

5 DISCUSSION

A set of Middle Devonian pillow lavas from the Rhenish Massif was assessed in this palaeomagnetic study. All samples are considered to have formed simultaneously and therefore they should contain similar palaeomagnetic directions and intensities. Furthermore, remagnetization processes are likely to have affected all rocks to the same extent, as they are from a ∼100 m wide area and of similar composition. Although the rock-magnetic experiments show evidence for the presence of common palaeomagnetic recorders [i.e. fine-grained magnetite as evidenced by the presence of Hopkinson peaks (Figs 3e–h; Fig. D2, Appendix D)], the obtained palaeomagnetic directions are enigmatic. There is a clear difference in demagnetization behaviour depending on demagnetization strategy used (AF, thermal or a combination of these). Thermal and AF + thermal demagnetization strategies show demagnetization paths along great circles that could be explained by a combination of a Kiaman and present-day field overprint. However, these overprints are not easily identified in all samples and we cannot exclude that a trace of a Devonian magnetization is still present in the rocks. Only one sample yields an interpretable palaeointensity that indicates an ultralow palaeomagnetic field.

5.1 Rock-magnetism

It is atypical for demagnetization experiments on volcanic rocks to not result in reliable palaeomagnetic directions. An explanation for the atypical directional results could be the low initial magnetization

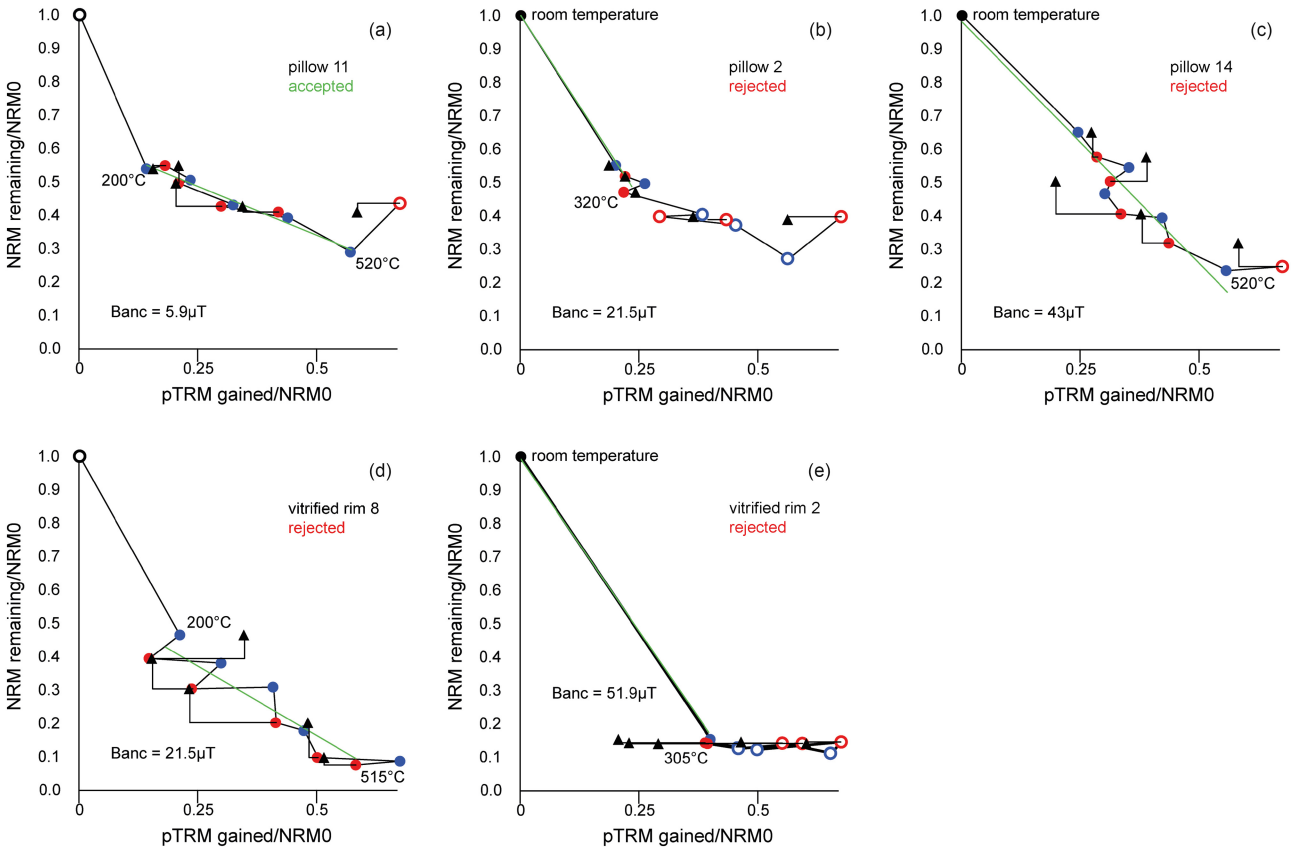

Figure 7. The five Thellier-type experiments carried out using the IZZI-protocol, with a B_{lab} of 10 μT, passing some selection criteria. (a)–(c) on whole rock specimens (d)–(e) and on vitrified rims. The remaining NRM (vertical axis) and the pTRM gained (horizontal axis) are normalized to the original NRM (NRM0) of the specimens. Red and blue circles indicate the data of the IZ- and ZI-field measurements, respectively. Triangles indicate pTRM checks and the green line is the linear regression trendline through the selected data. (a) A specimen from pillow 11 shows the only successful bulk rock result in a high-temperature segment (200–520 °C). The obtained palaeointensity is 5.9 μT. (b) A field of 21.5 μT was determined in the temperature range 20–280 °C for a specimen of pillow 2. This result includes the room temperature step and is therefore rejected as a primary palaeointensity. (c) A field of 43.0 μT was determined in the temperature range 20–520 °C for a specimen of pillow 14. This result includes the room temperature step and is therefore rejected as a primary palaeointensity. (d) The vitrified rim of pillow 8 has a palaeointensity of 21.5 μT. This result is rejected, because of the non-ideal strong zigzagging behaviour and high β-value indicative of MD behaviour. (e) A field of 51.9 μT was determined in the temperature range 20 –270 °C for a vitrified rim of pillow 2. This result includes the room temperature step and is therefore rejected as a primary palaeointensity.

values of our samples. Typically, pillow basalts hold a magnetization larger than 1 A m^{-1}, but we found values in the order of magnitudes from 1×10^{-2} to 1 A m^{-1}. These values are unexpectedly low for a basaltic rock that forms under typical present-day geomagnetic field conditions (e.g. Johnson & Hall 1978; Gee & Kent 1997).

To determine why these values are low, we studied the rock-magnetic properties of the pillow basalts. The main magnetic carrier in the rocks is primary (Ti-)magnetite (Figs 3a–h) and is a mixture of (P)SD and MD grains (Fig. 3m). The coercivities are low, due to the MD grains present in the samples (Figs 3j–l). IRM acquisition curves show that the magnetic recorders are indeed capable of recording high magnetizations (Fig. 3i). Although the amount of MD grains is not ideal for palaeointensity experiments, we would at least expect interpretable directional results from these magnetic recorders as (P)SD grains usually contain the majority of the magnetization in volcanic rocks. The demagnetization curves (Figs 5c and f) show that the majority of the NRM is lost at low coercivities (<10 mT) and low temperatures (<250 °C), which is not expected for typical (Ti-)magnetite. The combination of the high amount of MD grains and the low initial magnetization values of the samples might suggest that the (P)SD grains are not retaining a magnetization in the samples. We hypothesize that the basalts likely contain a mixture of SD/PSD and MD grains, but that the magnetic signal in our measurements is dominated by MD grains, which are easily (re-)magnetized in ambient fields. Commonly, the magnetic signal of the MD grains is overwhelmed by the signal from (P)SD grains, but in the case of the Middle Devonian pillow basalts, the (P)SD grains have possibly not recorded a magnetic field, and the signal is thus dominated by the MD grains. Therefore, the directional results might represent pronounced viscous behaviour of the MD grains. Viscous behaviour was also observed during repeated NRM measurements over a time of several weeks, while the samples were stored in a stable lab field.

5.2 Remagnetization

While Devonian rocks commonly display evidence of significant to pervasive overprinting by younger magnetic fields (van der Boon *et al.* 2022 and references therein), predominantly the Kiaman superchron, we struggle to explain our results by overprinting. While we lack field tests to constrain that our demagnetization results are Devonian in age, the lack of a full resemblance to younger palaeomagnetic poles partly precludes a remagnetization scenario.

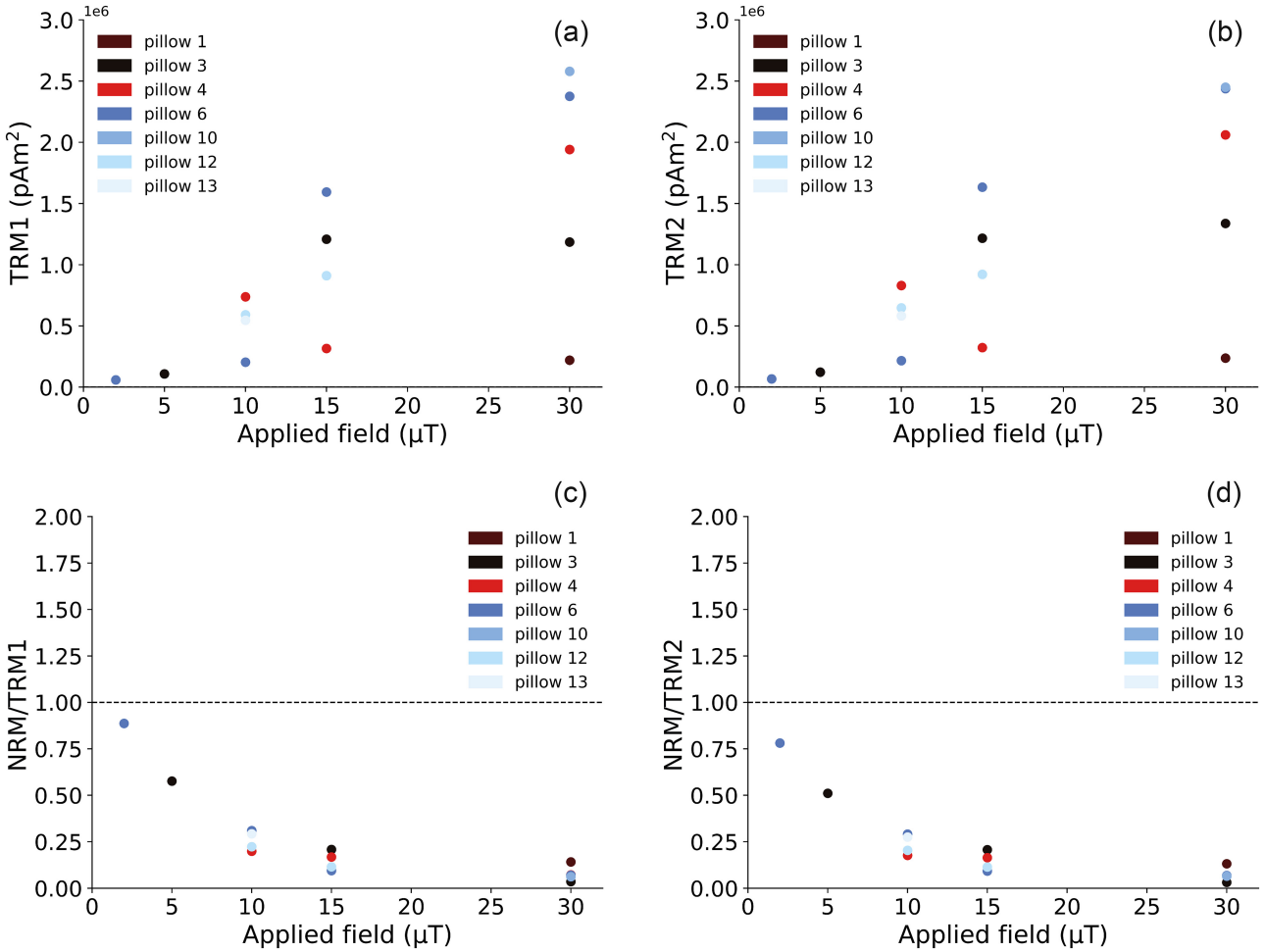

Figure 8. (a)–(b) A full TRM was imparted by cooling from 615 °C at five different magnetic field strengths. This procedure was done twice, to ensure reproducibility without (major) alteration. Specimens with a large change in susceptibility (see Chapter 3.4.2) were omitted and are not shown in these plots. In general, as prescribed by theory, a TRM induced in a stronger field is higher. (c)–(d) When dividing the NRM by the obtained TRM, a decreasing trend is observed with increasing field. The dashed line indicates NRM/TRM equals 1, which would be expected if the imparted field is close to the field experienced by the pillow basalts when they formed. An applied field of 2–5 μT results in a ratio closest to this value.

Viscous multidomain behaviour influences the low coercivity component (Fig. 6a) and might explain the observed high mean inclination in this analysis. The low-temperature components (Figs 6d and g) can be tentatively explained by a present-day magnetic field overprint. The high coercivity and high-temperature components (Figs 6b, e, h) result in similar declinations but show lower inclinations, these could potentially be a Devonian direction. However, when great circle analysis is applied to the thermal data (Fig. 6f), we find the results plotting as great circles between Kiaman and present-day field directions, which points to a combination of Kiaman and present-day field remagnetization in our samples. Although the AF demagnetization behaviour is univectorial and does not show demagnetization paths along great circles, we suggest that the directions we obtained could result from a combination of Kiaman and present-day field directions, since the means of the high coercivity components (Fig. 6c) are similar to the direction of the thermal demagnetization great circles. The great circle fitting of the AF + thermal demagnetization (Fig. 6i) experiments results in a slightly rotated mean. This could be the result of a present-day field direction and Kiaman direction in combination with a tectonic rotation. Another explanation could be the combination of a Devonian direction with a present-day overprint, although this option cannot be further constrained. Nonetheless, an overprinting mechanism is needed to explain a (partial) remagnetization in our samples.

A chemical remanent magnetization (CRM) is a secondary remanence that affects magnetic minerals by chemical alteration at temperatures below their Curie point in the presence of a magnetic field. Although chloritization is present in our samples, it is believed that this occurred almost instantaneously when the pillows were formed due to sea water interaction with the hot basalts (Wedepohl *et al.* 1983; Von Raumer *et al.* 2017). Iron ore formation in the region was contemporaneous with the volcanism (von Raumer *et al.* 2017), and we can thus exclude this ore formation as a cause for later overprinting. Later, only very low-grade metamorphism occurred during the Variscan orogeny (Moe 2000). It is therefore difficult to explain the Kiaman overprint with a CRM, since no substantial later alteration is found in the rocks. Furthermore, if a Kiaman CRM would be present, we fail to explain why Kiaman directions are not well-resolved in our data set.

A thermoviscous remanent magnetization (TVRM) could reset the primary magnetization in the rocks if high temperatures are reached for a significant amount of time. From the conodont alteration index, a maximum temperature of 250–300 °C is determined (Ahrendt *et al.* 1983), which is again argued to have been reached

almost instantaneously during the formation of the pillow lavas. It is therefore difficult to explain the Kiaman overprint with this mechanism.

A viscous remanent magnetization (VRM) can be acquired by magnetic minerals residing in a magnetic field for a sufficient amount of time. This can alter the natural remanent magnetization state. Particularly samples that have a low initial magnetization state such as our samples, are prone to acquiring a VRM. PSD grains are least sensitive to acquiring a VRM, compared to both SD grains close to the SP threshold and MD grains (Yu & Tauxe 2006). This mechanism may explain the present-day field and Kiaman overprints in the samples. However, we do not find these overprints in all samples and the overprints can only tentatively be found with great circle analysis. Differences in magnetic grain size might partly explain this behaviour. Tauxe & Love (2003) describe viscous magnetizations in submarine basalts, however these are dominated by low blocking temperatures and TM60. Our samples are not directly comparable to theirs.

Although we find evidence of overprints in our samples, it is difficult to explain the overprinting mechanism behind it. The conditions for remagnetization are barely met. Particularly, we consider it likely that an overprint that was acquired either as a CRM or TVRM during the Kiaman would have resulted in magnetizations that are stronger than the ones we observe in our samples, and with a clear Kiaman direction. Since we do not find full Kiaman or present-day overprints in the samples, this suggests that at least part of the original NRM is intact. However, we cannot derive a Devonian direction with certainty from this potentially primary TRM. A possible explanation could be a very weak original NRM, or even the lack of an original NRM in the samples.

Although part of the directional data can be explained by remagnetization, several scenarios could contribute to scattered palaeodirections. Large spreads in directions have been previously observed in Devonian lava sequences (Bazhenov *et al.* 2013; Hawkins *et al.* 2019), which has been explained as a result of strongly increased secular variation of the Devonian geomagnetic field. A tectonic scenario can be excluded as an explanation for the large spread in directions, since the pillows come from a single block, and the data spread is present within the individual pillows as well.

Besides Kiaman and present-day remagnetization, we considered other overprinting mechanisms. The presence of anisotropy (Fig. 4) might explain part of the scatter in the directional data. However, our ChRM distribution spans inclinations of 0°–89° and has a widespread in declination. The AMS alone can never be a full explanation for such ambiguous directional data. Furthermore, the spread in AMS values is not consistent within the pillows nor are the Pj-values related to the measured directions (Fig. C1, Appendix C).

5.3 Middle Devonian magnetic field

Our accepted palaeointensity estimate of 5.9 μT (bulk rock; Fig. 7a) points towards an ultralow palaeointensity of the geomagnetic field during the Middle Devonian. The low success rate of the palaeointensity experiments raises the question whether the pillow basalts are poor recorders of the magnetic field or whether the magnetic field had an unusual configuration causing the lack of a magnetization in the pillows. Were the pillows originally magnetized and was the magnetization later removed? Or were they initially not magnetized and is it therefore problematic to retrieve reliable palaeointensities?

From the rock-magnetic perspective, the pillows are expected to be reasonably good recorders of the magnetic field and we would anticipate being able to retrieve meaningful palaeointensities with the applied IZZI-protocol. The main magnetic recorder is (Ti-)magnetite, and a minor amount of maghemite is present in some samples (Figs 3a–d). Alteration of the magnetic minerals in susceptibility versus temperature experiments starts above 350–400 °C, indicating that pTRM checks will likely start to fail only above these temperatures (Figs 3e–h). MD and PSD grains are dominant both in the bulk rock as well as in the vitrified rims (Fig. 3m). Smaller magnetic grain sizes in glassy or vitrified rims are expected to lead to successful palaeointensity results (Carlut & Kent, 2002; Selkin & Tauxe 2000; Tauxe & Love 2003). Although the presence of MD grains is not ideal, samples containing mainly PSD grains should at least have a detectable magnetization. Cych *et al.* (2024) use micromagnetic modelling to demonstrate that the range of size, shape and composition of unstable magnetic carriers is large. Particularly titanomagnetite of intermediate composition, both prolate and oblate in shape, has a large range of sizes over which it is magnetically unstable. Although our magnetite composition is typically TM15-TM25 and has a lower titanium content than TM30-40, which is unstable over the largest size range (Cych *et al.* 2024), this difference could still contribute to the failure of most of our palaeointensity experiments.

Since no obvious remagnetization mechanism could be identified, we could argue that the obtained palaeointensity is held by a primary TRM. However, since partial overprints have been identified in the directional results, we could also argue that the intensities are the result of a VRM overprint.

In the first case, the obtained palaeointensity suggests a weak to ultraweak palaeomagnetic field during the Middle Devonian, which is in line with findings of other studies (van der Boon *et al.* 2022 and references therein). However, if we deem the samples remagnetized by a VRM, we cannot accept the value of 5.9 μT as a Devonian palaeointensity. Since a TRM is a more efficient mechanism than a VRM to impart a magnetization, the obtained palaeointensity value can then only be considered a minimum value for the palaeofield during remagnetization. However, we argue if a large primary magnetization would have been present, we should find traces that overcome this low value. We therefore suggest that the magnetic field in which the palaeointensity was recorded was likely weak on both occasions.

The obtained palaeointensity result, along with the fidelity test of the NRM recording and the overall lack of solid palaeodirectional results, supports the suggestion of an (ultra-)weak geomagnetic field. This aligns with the findings of Bellon *et al.* (2025), who suggest that an ultralow field (<2 μT) does not easily produce interpretable paleodirections in vortex-state magnetite. Such an ultralow magnetic field could be the result of a geomagnetic field not dominated by a geocentric axial dipole (GAD).

6 CONCLUSION

The pillow lavas of the Philippstein volcano in the Rhenish Massif offer an opportunity to study the geomagnetic field of the Middle Devonian. However, it appears to be complicated to retrieve sensible palaeomagnetic directions. With univectorial low-coercivity and low-temperature components we find traces of a present-day field overprint in the samples. However, at high coercivities or temperatures we do not find univectorial results. With the use of great circle analyses we suggest that a combination of a present-day field overprint and a Kiaman overprint could be present. Although Kiaman overprints are common in Devonian rocks, full Kiaman directions are never uncovered in our samples. We are therefore hesitant to

claim that all results are convincingly explained with both these overprints. No clear Middle Devonian direction can be retrieved either. In any case, our rocks are weakly magnetized and palaeointensity experiments indicate potential low magnetic field values. Since we cannot explain the lack of a magnetization with rock-magnetic properties or an obvious remagnetization mechanism, we suggest a low intensity or non-dipolar magnetic field might have prevailed during (part of) the Middle Devonian.

ACKNOWLEDGMENTS

We thank Wilhelm Jost GmbH & Co. for facilitating access to the Philippstein quarry. Sofie Hildegard Ryen is thanked for her help with demagnetization experiments. This research is part of project PANDA, financed by the Research Council of Norway through its Young Talent scheme (project number 3346220). AvdB also acknowledges financial support from the Research Council of Norway through its Centers of Excellence scheme, project number 332523 (PHAB). This project has received funding from the European Research Council (ERC) under the European Union's Horizon 2020 research and innovation program (Grant agreement No. 851460 to LVdG). Shuhui Cai and an anonymous reviewer are gratefully acknowledged for their thorough reviews that improved the manuscript.

DATA AVAILABILITY

Palaeodirectional data is available under Data DOI 10.7288/V4/MAGIC/20238. Palaeointensity data is available under Data DOI 10.7288/V4/MAGIC/20239.

REFERENCES

Ahrendt, H., Clauer, N., Hunziker, J.C. & Weber, K., 1983. Migration of folding and metamorphism in the R(h)einische Schiefergebirge deduced from K-Ar and Rb-Sr age determinations, *Intracont. Fold Belts,* 323–338.

Alken, P. *et al.* 2021. International geomagnetic reference field: the thirteenth generation, *Earth Planets Space,* **73**(1), 1–25.

Bazhenov, M.L., Van der Voo, R., Levashova, N.M. & Dominguez, A.R., 2013. Late devonian palaeomagnetism of the North Tien Shan, Kyrgyzstan: can secular variation vary on a short timescale?, *Geophys. J. Int.,* **193**(2), 635–649.

Becker, R.T., Marshall, J.E.A., Da Silva, A.C., Agterberg, F.P., Gradstein, F.M. & Ogg, J.G., 2020. The devonian period, in *Geologic Time Scale 2020,* eds, Gradstein, F.M., Ogg, J.G., Schmitz, M.D. & Ogg, G.M., Elsevier, 733–810.

Béguin, A., Paterson, G.A., Biggin, A.J. & de Groot, L.V., 2020. Paleointensity. Org: an online, open source, application for the interpretation of paleointensity data, *Geochem. Geophys. Geosyst.,* **21**(5), e2019GC008791, doi:10.1029/2019GC008791.

Bellon, U.D., Williams, W., Muxworthy, A.R., Junior, G.F.S., Nagy, L., Uieda, L. & Trindade, R.I., 2025. Efficiency of thermoremanent magnetization acquisition in vortex-state particle assemblies, Authorea Preprints. *Geophys. Res. Lett.,* **52**(8), e2025GL114771.

Biggin, A.J. & Paterson, G.A., 2014. A new set of qualitative reliability criteria to aid inferences on palaeomagnetic dipole moment variations through geological time, *Front. Earth Sci.,* **2,** 24, doi:10.3389/feart.2014.00024.

Bono, R.K., Paterson, G.A. & Biggin, A.J., 2022b. MCADAM: a continuous paleomagnetic dipole moment model for at least 3.7 billion years, *Geophys. Res. Lett.,* **49**(21), e2022GL100898, doi:10.1029/2022GL100898.

Bono, R.K., Paterson, G.A., van der Boon, A., Engbers, Y.A., Michael Grappone, J., Handford, B. & Biggin, A.J., 2022a. The PINT database: a definitive compilation of absolute palaeomagnetic intensity determinations since 4 billion years ago, *Geophys. J. Int.,* **229**(1), 522–545.

Carlut, J. & Kent, D.V., 2002. Grain-size-dependent paleointensity results from very recent mid-oceanic ridge basalts, *J. geophys. Res.: Solid Earth,* **107**(B3), EPM 2–1-2-12, doi: 10.1029/2001JB000439.

Cromwell, G., Tauxe, L., Staudigel, H. & Ron, H., 2015. Paleointensity estimates from historic and modern Hawaiian lava flows using glassy basalt as a primary source material, *Phys. Earth planet. Inter.,* **241,** 44–56.

Cych, B., Paterson, G.A., Nagy, L., Williams, W. & Moskowitz, B., 2024. Magnetic domain states and critical sizes in the titanomagnetite series, *J. geophys. Res.: Solid Earth,* **129**(6), e2024JB028805, doi:10.1029/2024JB028805.

Dekkers, M.J. & Böhnel, H.N., 2006. Reliable absolute palaeointensities independent of magnetic domain state, *Earth planet. Sci. Lett.,* **248**(1-2), 508–517.

Driscoll, P.E., 2016. Simulating 2 Ga of geodynamo history, *Geophys. Res. Lett.,* **43**(11), 5680–5687.

Dunlop, D.J. & Özdemir, Ö., 1997. In: *Rock Magnetism: Fundamentals and Frontiers (No. 3)*. Cambridge Univ. Press.

Epstein, A.G., Epstein, J.B. & Harris, L.D., 1977. Conodont color alteration; an index to organic metamorphism (No. 995), *US Govt. Print. Off.,* 1–27.

Fabian, K. & Leonhardt, R., 2010. Multiple-specimen absolute paleointensity determination: an optimal protocol including pTRM normalization, domain-state correction, and alteration test, *Earth planet. Sci. Lett.,* **297**(1-2), 84–94.

Finn, D.R. & Coe, R.S., 2016. A new protocol for three-axis static alternating field demagnetization of rocks, *Geochem. Geophys. Geosyst.,* **17**(5), 1815–1822.

Flick, H., Lippert, H.J., Nesbor, H.D. & Requadt, H., 1988. Lahn- und Dillmulde, In: *Geologie und Hydrothermale Mineralisationen im Rechtsrheinischen Schiefergebirge,*pp. 33–62, ed. Kirnbauer, T., (Hrsg.) Jahrbuch Nassauischer Verein für Naturkunde, Sonderband 1.

Flick, H. & Nesbor, H.D., 1988. Der Vulkanismus in der Lahnmulde, *Jahresber. Mitteilungen Oberrheinischen Geol. Ver.,* **70,** 411–475.

Flick, H., Nesbor, H.D. & Behnisch, R., 1990. Iron ore of the Lahn-Dill type formed by diagenetic seeping of pyroclastic sequences—A case study on the Schalstein section at Gänsberg (Weilburg), *Geol. Rundsch.,* **79,** 401–415.

Franke, W., 2000. The mid-European segment of the Variscides: tectonostratigraphic units, terrane boundaries and plate tectonic evolution, *Geol. Soc. London, Special Publ.,* **179**(1), 35–61.

Franke, W., Huckriede, H., O'Sullivan, P. & Wemmer, K., 2019. Zircons to the front: accretionary history of the Rheno-hercynian active margin (Variscides, Germany), *Can. J. Earth Sci.,* **56**(12), 1375–1397.

Gee, J. & Kent, D.V., 1997. Magnetization of axial lavas from the southern East Pacific Rise (14–23 S): geochemical controls on magnetic properties, *J. geophys. Res.: Solid Earth,* **102**(B11), 24 873–24 886.

Golonka, J., 2020. Late devonian paleogeography in the framework of global plate tectonics, *Global Planet. Change,* **186,** 103129, doi:10.1016/j.gloplacha.2020.103129.

Green, T. *et al.* 2021. High-resolution late devonian magnetostratigraphy from the Canning Basin, Western Australia: a re-evaluation, *Front. Earth Sci.,* **9,** 757749, doi:10.3389/feart.2021.757749.

Hansma, J. *et al.* 2015. Late devonian carbonate magnetostratigraphy from the Oscar and Horse Spring Ranges, Lennard Shelf, Canning Basin, Western Australia, *Earth planet. Sci. Lett.,* **409,** 232–242.

Hawkins, L.M. *et al.* 2021. Intensity of the Earth's magnetic field: evidence for a mid-paleozoic dipole low, *Proc. Natl. Acad. Sci.,* **118**(34), doi:10.1073/pnas.2017342118.

Hawkins, L.M.A., Anwar, T., Shcherbakova, V.V., Biggin, A.J., Kravchinsky, V.A., Shatsillo, A.V. & Pavlov, V.E., 2019. An exceptionally weak devonian geomagnetic field recorded by the Viluy Traps, Siberia, *Earth planet. Sci. Lett.,* **506,** 134–145.

Jeleńska, M., Kądziałko-Hofmokl, M., Bakhmutov, V., Poliachenko, I. & Ziółkowski, P., 2014. Palaeomagnetic and rock magnetic study of lower devonian sediments from Podolia, SW Ukraine: remagnetization problems, *Geophys. J. Int.,* **200**(1), 557–573.

Johnson, H.P. & Hall, J.M., 1978. A detailed rock magnetic and opaque mineralogy study of the basalts from the Nazca Plate, *Geophys. J. Int.,* **52**(1), 45–64.

Kaiser, S.I., Aretz, M. & Becker, R.T., 2016. The global Hangenberg Crisis (devonian-carboniferous transition: review of a first-order mass extinction, in *Devonian Climate, Seal Level and Evolutionary Events, Vol. 432,* pp. 387–437, eds, Becker, R.T., Königshof, P. & Brett, C.E., Geological Society of London, Special Publication.

Kirschvink, J.L., 1980. The least-squares line and plane and the analysis of palaeomagnetic data, *Geophys. J., Royal Astronomical Society,* **62**(3), 699–718.

Königshof, P. & Flick, H., 2024. Fringing reef growth in the Mid-Devonian: an example from the southern Rhenish Massif, Germany, *Palaeobiod. Palaeoenviron.,* **104,** doi: 10.1007/s12549-023-00591-1.

Königshof, P., Loos, S. & Rutkowski, J., 2024. Lithofacies variability and facies analysis of a Givetian reef in the southwestern Lahn Syncline (Rhenish Massif, Germany), *Palaeobiod. Palaeoenviron.,* **104,** 461–491, doi: 10.1007/s12549-023-00585-z.

Königshof, P., Nesbor, H.D. & Flick, H., 2010. Volcanism and reef development in the Devonian: a case study from the Lahn syncline, Rheinisches Schiefergebirge (Germany), *Gondwana Res.,* **17**(2-3), 264–280, doi: 10.1016/j.gr.2009.09.006.

Koymans, M.R., Langereis, C.G., Pastor-Galán, D. & van Hinsbergen, D.J., 2016. Paleomagnetism. Org: an online multi-platform open source environment for paleomagnetic data analysis, *Comput. Geosci.,* **93,** 127–137.

Koymans, M.R., Van Hinsbergen, D.J.J., Pastor-Galán, D., Vaes, B. & Langereis, C.G., 2020. Towards FAIR paleomagnetic data management through paleomagnetism. Org 2.0, *Geochem. Geophys. Geosyst.,* **21**(2), e2019GC008838.

Lippert, H.J. & Flick, H., 1998. Vulkano-sedimentäre Roteisenerze vom Lahn-Dill-Typ. Geologie und hydrothermale mineralisationen im rechtsrheinischen Schiefergebirge, *Nassauischer Verein für Naturkunde, Wiesbaden, Sonderband,* **1,** 121–128.

Marcilly, C.M., Torsvik, T.H. & Conrad, C.P., 2022. Global phanerozoic sea levels from paleogeographic flooding maps, *Gondwana Res.,* **110,** 128–142.

Maxbauer, D.P., Feinberg, J.M. & Fox, D.L., 2016. MAX UnMix: a web application for unmixing magnetic coercivity distributions, *Comput. Geosci.,* **95,** 140–145.

McFadden, P.L. & McElhinny, M.W., 1988. The combined analysis of remagnetization circles and direct observations in palaeomagnetism, *Earth planet. Sci. Lett.,* **87**(1-2), 161–172.

Meisl, S., 1995. Igneous activity, in *Pre-Permian Geology of Central and Eastern Europe,* pp. 118–131, eds Dallmeyer, R.D., Franke, W. & Weber, K., Springer.

Merrill, R.T., McElhinny, M.W. & McFadden, P.L., 1998. *The Magnetic Field of the Earth: Paleomagnetism, the Core, and the Deep Mantle. 63,* Academic Press.

Moe, A., 2000. Structural development of a volcanic sequence of the Lahn area during the variscan orogeny in the Rhenohercynian Belt (Germany), [Doctoral dissertation, Heidelberg University]. HeiDOK.

Mullender, T.A., Frederichs, T., Hilgenfeldt, C., de Groot, L.V., Fabian, K. & Dekkers, M.J., 2016. Automated paleomagnetic and rock magnetic data acquisition with an in-line horizontal "2 G" system, *Geochem. Geophys. Geosyst.,* **17**(9), 3546–3559.

Mullender, T.A.T., Van Velzen, A.J. & Dekkers, M.J., 1993. Continuous drift correction and separate identification of ferrimagnetic and paramagnetic contributions in thermomagnetic runs, *Geophys. J. Int.,* **114**(3), 663–672.

Nesbor, H.D., 2007. Paläozoischer Vulkanismus im Lahn–Dill-Gebiet–südöstliches Rheinisches Schiefergebirge (Exkursion E am 12. April 2007), *Jber. Mitt. oberrhein. geol. Ver., N.F,* **89,** 193–216.

Nesbor, H.D., 2019. Alpinotype Deckentektonik im Rheinischen Schiefergebirge (Exkursion I am 26. April 2019), *Jber. Mitt. oberrhein. geol. Ver., N.F,* **101,** 197–226.

Pastor-Galán, D., Ursem, B., Meere, P.A. & Langereis, C., 2015. Extending the Cantabrian orocline to two continents (from Gondwana to Laurussia), Paleomagnetism from South Ireland., *Earth planet. Sci. Lett.,* **432,** 223–231.

Paterson, G.A., Tauxe, L., Biggin, A.J., Shaar, R. & Jonestrask, L.C., 2014. On improving the selection of Thellier-type paleointensity data, *Geochem. Geophys. Geosyst.,* **15**(4), 1180–1192.

Rejebian, V.A., Harris, A.G. & Huebner, J.S., 1987. Conodont color and textural alteration: an index to regional metamorphism, contact metamorphism, and hydrothermal alteration, *Geol. Soc. Am. Bull.,* **99**(4), 471–479.

Schnapperelle, S., Kachelrieß, G., Kühn, R., Methner, S., Schulz, C. & Mertmann, D., 2021. Devonischer Vulkanismus und Sedimentation im Gebiet Padberg und Giershagen, NE Rheinisches Schiefergebirge, *Hallesches Jahrbuch für Geowissenschaften,* **44,** 7–43.

Schulz-Isenbeck, J., Bröcker, M. & Berndt, J., 2019. U–Pb zircon dating of paleozoic volcanic rocks from the Rheno-Hercynian Zone: new age constraints for the Steinkopf formation, Lahn-Dill area, Germany, *Int. J. Earth Sci.,* **108,** 1835–1855.

Selkin, P.A. & Tauxe, L., 2000. Long-term variations in palaeointensity, *Phil. Trans. R. Soc. London. Ser. A: Math. Phys. Eng. Sci.,* **358**(1768), 1065–1088.

Shatsillo, A.V. & Pavlov, V.E., 2019. Systematics of paleomagnetic directions from early–Middle devonian rocks of Minusa troughs: new data and old problems, *Izv. Phys. Solid Earth,,* **55,** 471–487.

Shcherbakova, V.V., Biggin, A.J., Veselovskiy, R.V., Shatsillo, A.V., Hawkins, L.M.A., Shcherbakov, V.P. & Zhidkov, G.V., 2017. Was the devonian geomagnetic field dipolar or multipolar? Palaeointensity studies of devonian igneous rocks from the Minusa Basin (Siberia) and the Kola Peninsula dykes, Russia, *Geophys. J. Int.,* **209**(2), 1265–1286.

Shcherbakova, V.V., Zhidkov, G.V., Shcherbakov, V.P., Golovanova, I.V., Danukalov, K.N. & Salmanova, R.Y., 2021. Ultra-low geomagnetic field intensity in the Devonian obtained from the southern ural Rock studies. Izvestiya, *Phys. Solid Earth,* **57**(6), 900–912.

Tauxe, L., Banerjee, S.K., Butler, R.F. & van der Voo, R., 2018. *Essentials of Paleomagnetism: Fifth Web Edition,* Scripps Institution of Oceanography.

Tauxe, L., Bertram, H.N. & Seberino, C., 2002. Physical interpretation of hysteresis loops: micromagnetic modeling of fine particle magnetite, *Geochem. Geophys. Geosyst.,* **3**(10), 1–22.

Tauxe, L. & Love, J.J., 2003. Paleointensity in Hawaiian scientific Drilling Project hole (HSDP2): results from submarine basaltic glass, *Geochem. Geophys. Geosyst.,* **4**(2), doi:10.1029/2001GC000276.

Tauxe, L. & Staudigel, H., 2004. Strength of the geomagnetic field in the cretaceous Normal Superchron: new data from submarine basaltic glass of the Troodos Ophiolite, *Geochem. Geophys. Geosyst.,* **5**(2), doi:10.1029/2003GC000635.

Thellier, E. & Thellier, O., 1959. On the intensity of the Earth's magnetic field in the historical and geological past, *Izv. Akad. Nauk SSSR, Ser. Geofiz,,* **9,** 1296–1331.

Torsvik, T.H. & Cocks, L.R.M., 2004. Earth geography from 400 to 250 ma: a palaeomagnetic, faunal and facies review, *J. Geol. Soc.,* **161,** 555–572.

Torsvik, T.H., Van der Voo, R., Preeden, U., Mac Niocaill, C., Steinberger, B., Doubrovine, P.V. & Cocks, L.R.M., 2012. Phanerozoic polar wander, palaeogeography and dynamics, *Earth-Sci. Rev.,* **114**(3-4), 325–368.

Valet, J.P., 2003. Time variations in geomagnetic intensity, *Rev. Geophys.,* **41**(1), doi:10.1029/2001RG000104.

van der Boon, A. *et al.* 2022. A persistent non-uniformitarian paleomagnetic field in the Devonian?, *Earth Sci. Rev.,* **231,** 104073, doi:10.1016/j.earscirev.2022.104073.

von Raumer, J.F., Nesbor, H.D. & Stampfli, G.M., 2017. The north-subducting Rheic Ocean during the Devonian: consequences for the Rhenohercynian ore sites, *Int. J. Earth Sci.,* **106**(7), 2279–2296.

Watkins, N.D. & Haggerty, S.E., 1967. Primary oxidation variation and petrogenesis in a single lava, *Contrib. Mineral. Petrol.,* **15,** 251–271.

Wedepohl, K.H., Meyer, K. & Muecke, G.K., 1983. Chemical composition and genetic relations of meta-volcanic rocks from the Rhenohercynian belt of northwest Germany, *Intracont. Fold Belts,* 231–256.

Yu, Y. & Dunlop, D.J., 2003. On partial thermoremanent magnetization tail checks in Thellier paleointensity determination, *J. geophys. Res.: Solid Earth,* **108**(B11), doi: 10.1029/2003JB002420.

Yu, Y. & Tauxe, L., 2006. Effect of multi-cycle heat treatment and pre-history dependence on partial thermoremanence (pTRM) and pTRM tails, *Phys. Earth planet. Inter.,* **157**(3-4), 196–207.

Yu, Y., Tauxe, L. & Genevey, A., 2004. Toward an optimal geomagnetic field intensity determination technique, *Geochem. Geophys. Geosyst.,* **5**(2), doi:10.1029/2003GC000630.

Zegers, T.E., Dekkers, M.J. & Bailly, S., 2003. Late carboniferous to permian remagnetization of Devonian limestones in the Ardennes: role of temperature, fluids, and deformation, *J. geophys. Res.: Solid Earth,* **108**(B7), doi:10.1029/2002JB002213.

Zijderveld, J.D.A., 1967, A.C. demagnetization of rocks: analysis of results, in *Methods in Paleomagnetism (254-286),* eds Collinson, D.W., Crees, K.M. & Runcorn, S.K., Elsevier.

Zwing, A. & Bachtadse, V., 2000. Paleoposition of the northern margin of Armorica in late devonian times: paleomagnetic and rock magnetic results from the Frankenstein Intrusive Complex (Mid-German Crystalline Rise), *J. geophys. Res.: Solid Earth,* **105**(B9), 21445–21456.

APPENDIX A—GRM

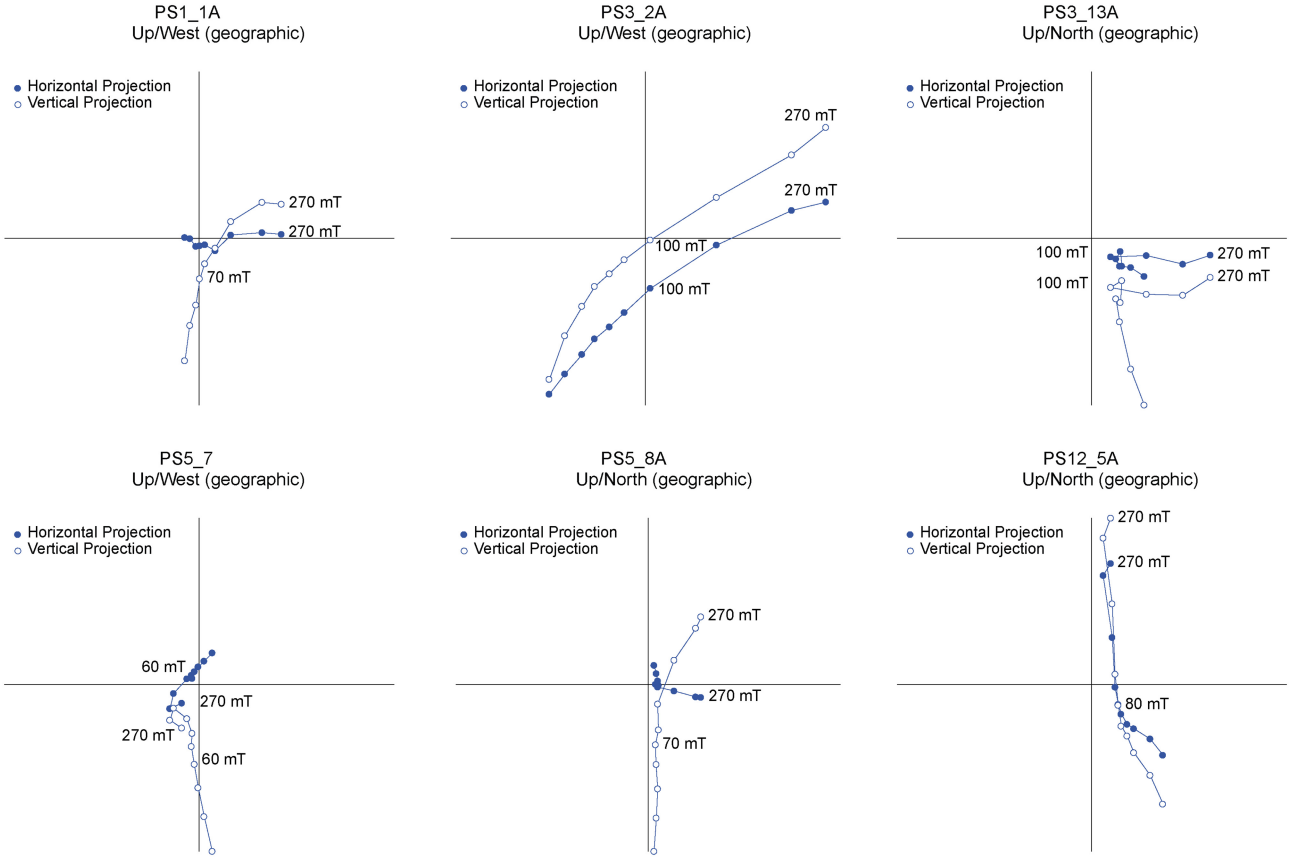

Figure A1. Examples of a GRM at high coercivities (>70 mT) during AF demagnetization experiments. At high coercivities, the demagnetization path moves away from the origin of the Zijderveld diagrams, indicating an induced GRM.

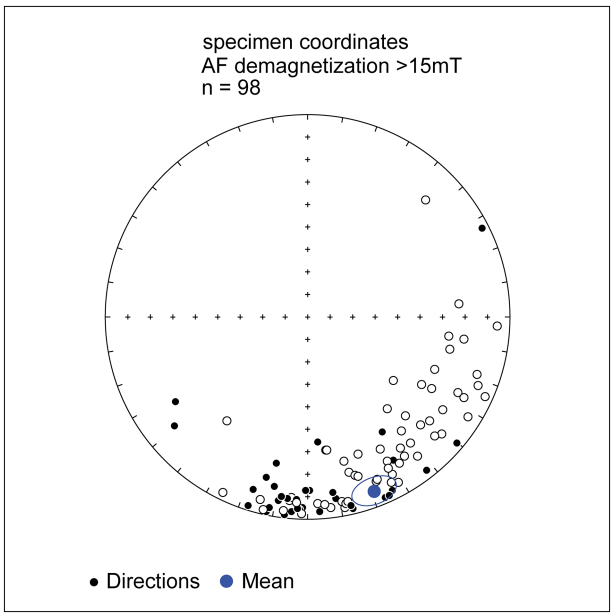

Figure A2. Specimen coordinates of AF > 15 mT demagnetization experiments. The last AF demagnetization axis in the Z-direction could lead to samples clustering perpendicular to this axis, on the great circle with inc = 0°. Although part of the samples tends to cluster around this low inclination value, there does not seem to be a clear GRM present throughout all samples.

APPENDIX B—IRM ACQUISITION CURVE UNMIXING

Appendix C—COMPARISON AMS AND DIRECTIONS

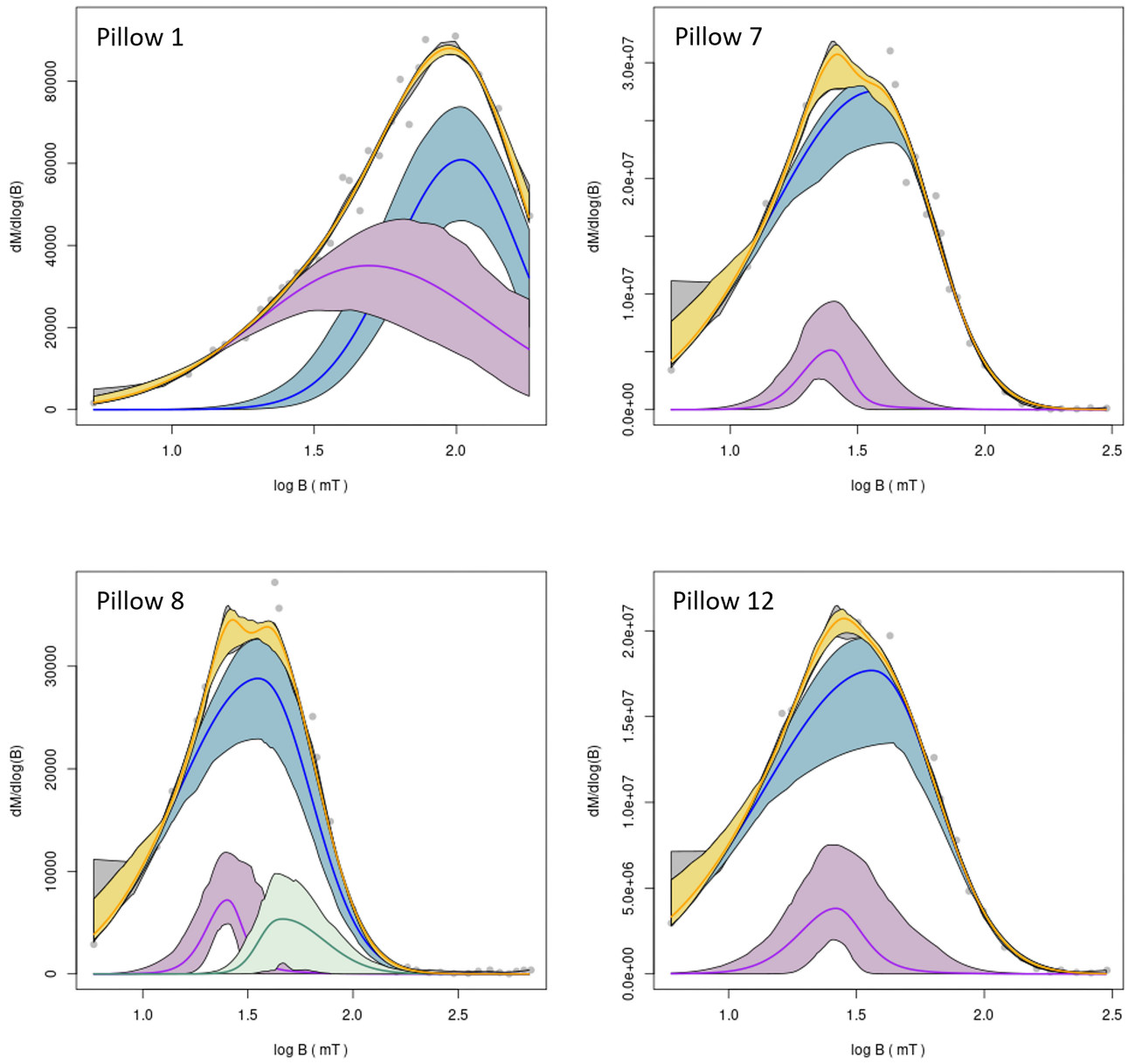

Figure B1. Unmixing of the IRM acquisition curves (Maxbauer *et al.* 2016) mainly indicates magnetite presence (Bh values of 1.36–1.74 log mT or 23–55 mT) and potentially high Ti-magnetite (Bh value of 2.00 log mT or 100 mT). The samples mainly contain one dominant magnetite population with a rather large DP value (0.23–0.35), indicating the presence of oxidized titanomagnetite. The small populations (<8 per cent) with typical Bh values of magnetite are likely a mathematical artefact of the fitting procedure, because small DP values are unlikely for magnetite populations in a basaltic lava.

APPENDIX D—ROCK-MAGNETISM

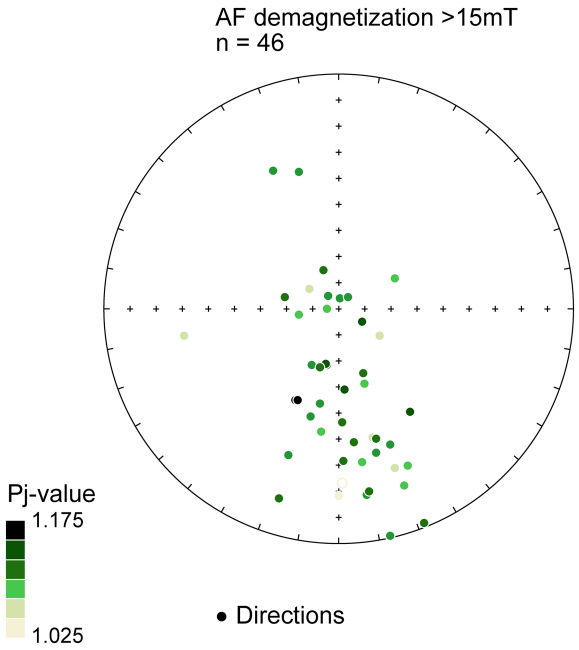

Figure C1. Pj-value of the AMS plotted per AF direction determined for high coercivity AF demagnetization experiments (Fig. 6b). There appears to be no relationship between Pj-value and declination or inclination.

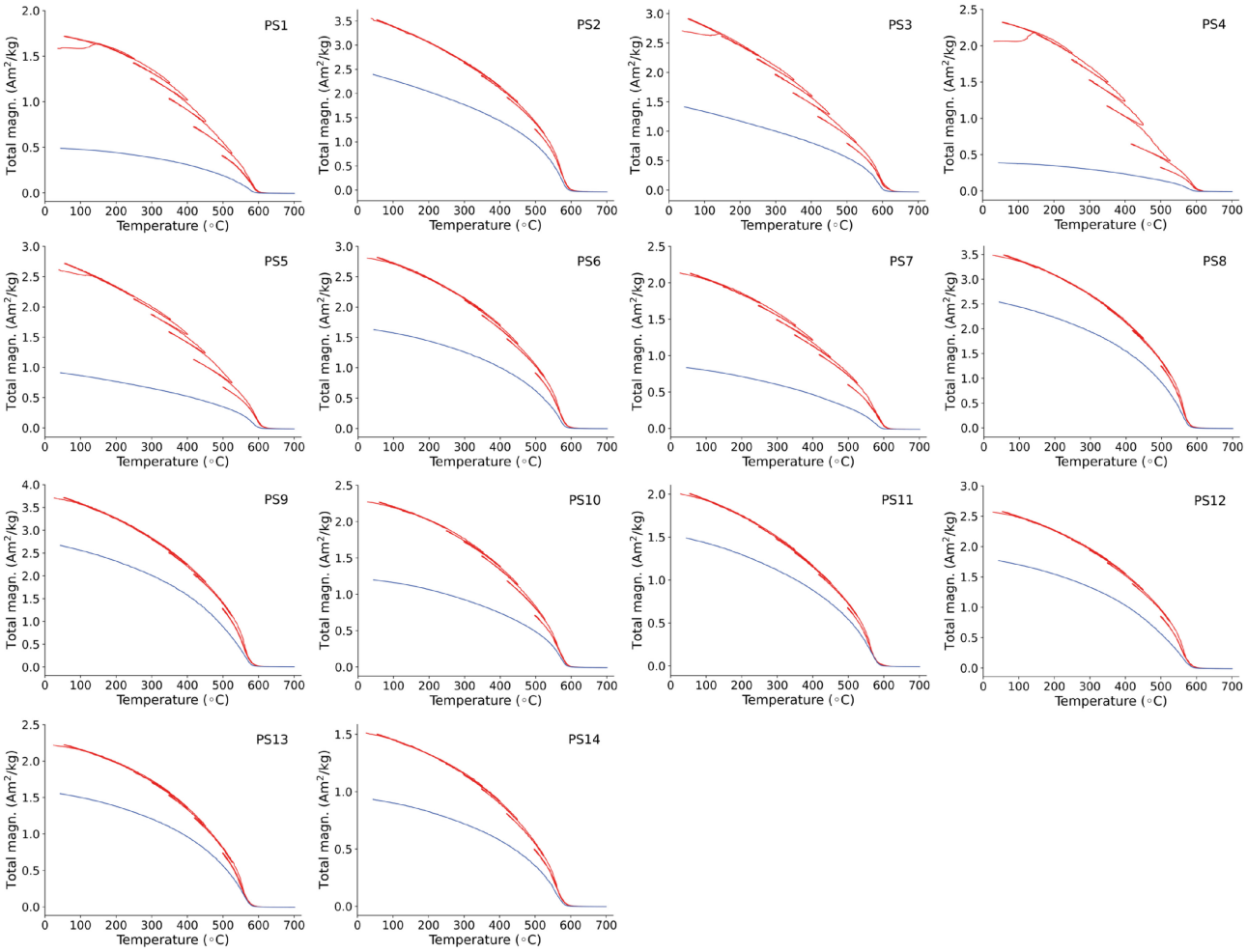

Figure D1. Magnetization versus temperature curves of all pillows.

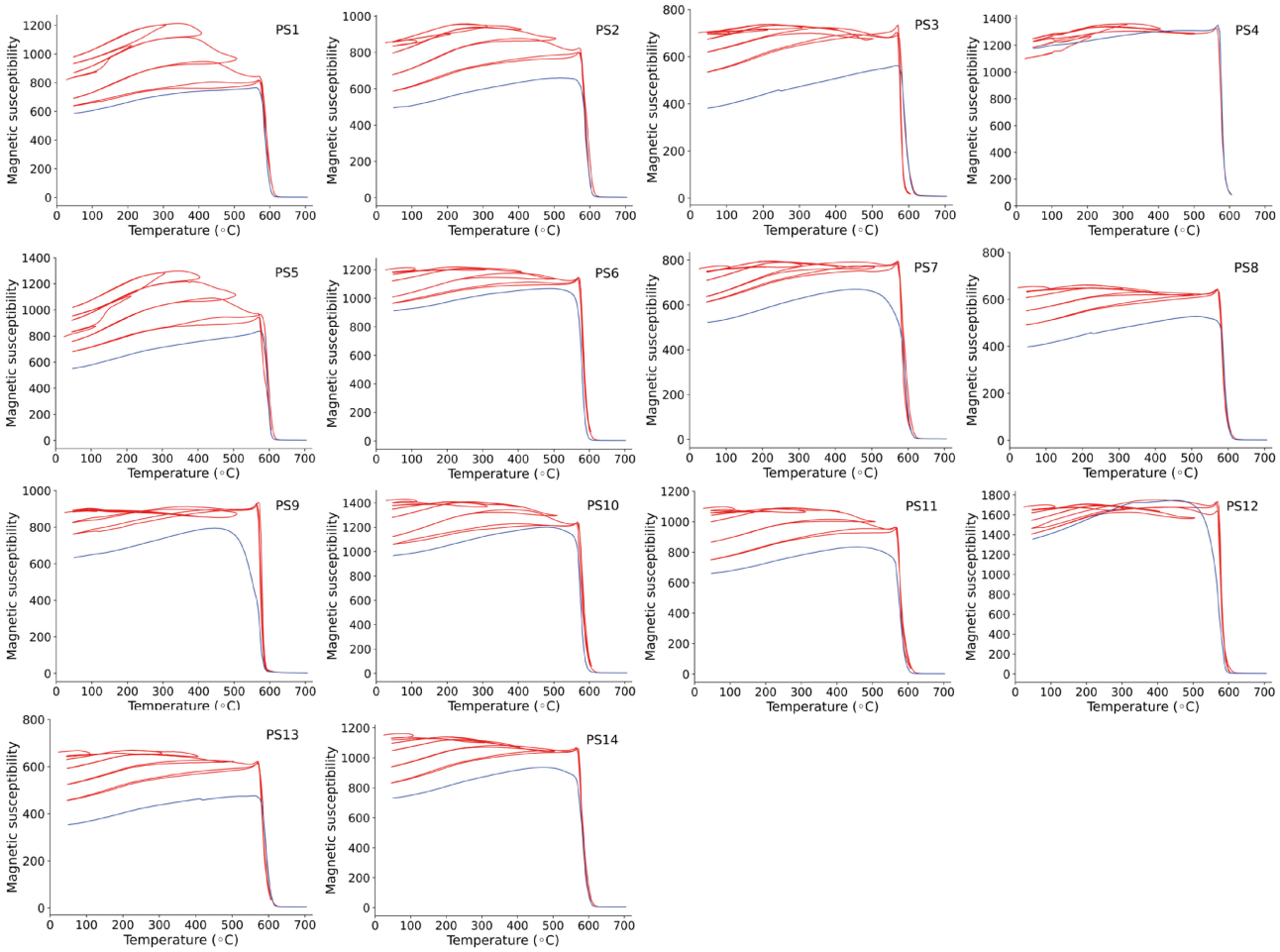

Figure D2. Susceptibility versus temperature curves of all pillows.

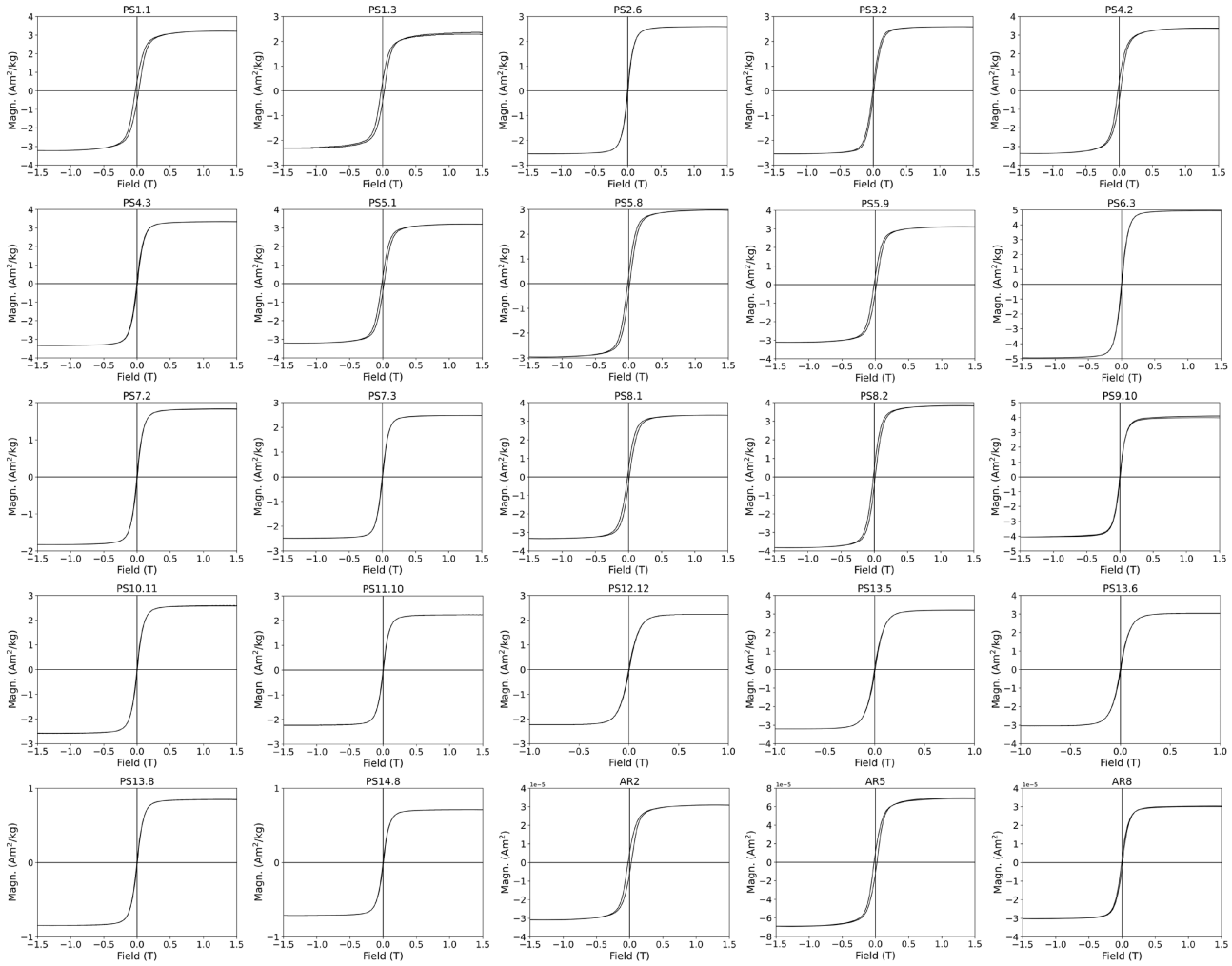

Figure D3. Slope-corrected hysteresis loops of all pillows (PS) and vitrified rims (AR).